Check for updates

Research Article

Received: 26 April 2024 Revised: 28 August 2024 Published online in Wiley Online Library:

(wileyonlinelibrary.com) DOI 10.1002/jctb.7759

Photocatalytic removal of aldrin and dieldrin using graphene oxide and TiO_2-doped $CuFe_2O_4$

Sevil Akçağlar*

Abstract

BACKGROUND: Conventional treatment processes and existing photocatalysts have proven insufficient in efficiently removing aldrin and dieldrin. Consequently, this study aimed to investigate the removal of aldrin and dieldrin from surface water using a titanium dioxide/graphene oxide/copper ferrite (TiO_2/GO/$CuFe_2O_4$) nanocomposite.

RESULTS: The highest photodegradation efficiencies for aldrin (100%) and dieldrin (99%) were achieved with a TiO_2/GO/$CuFe_2O_4$ nanocomposite dosage of 1.3 mg L^{-1}, at a sunlight intensity of 9 W m^{-2} and an optimal photodegradation time of 25 min. The maximum UV absorption wavelength of the TiO_2/GO/$CuFe_2O_4$ nanocomposite was observed at 365 nm. The quantum yield of the nanocomposite was recorded as 2.69×10^2 mol einstein^{-1}, and its bandgap energy was determined to be 3.31 eV. The first-order kinetic rate constants for aldrin and dieldrin were calculated as 0.05 and 0.047 min^{-1}, respectively. X-ray diffraction analysis confirmed the crystal structure of $CuFe_2O_4$/TiO_2, while Fourier transform infrared spectroscopy detected carboxylic, epoxy, carbonyl and other oxygenated groups within the TiO_2/GO/$CuFe_2O_4$ nanocomposite. Scanning electron microscopy and transmission electron microscopy images revealed that $CuFe_2O_4$ was situated on the outer layer of GO. Energy-dispersive X-ray analysis identified the elemental composition of the TiO_2/GO/$CuFe_2O_4$ nanocomposite as comprising GO, C, Cu, Fe, Ti and O. A reusability study demonstrated that the nanocomposite maintained excellent performance, achieving 99% removal efficiency after 79 cycles and 97% after 100 cycles.

CONCLUSIONS: The TiO_2/GO/$CuFe_2O_4$ nanocomposite effectively removed aldrin and dieldrin from surface water. This nanocomposite holds promise for the remediation of other aquatic ecosystems, such as bays, rivers and ocean waters.
© 2024 The Author(s). *Journal of Chemical Technology and Biotechnology* published by John Wiley & Sons Ltd on behalf of Society of Chemical Industry (SCI).

Keywords: aldrin; dieldrin; photocatalytic; TiO_2/GO/$CuFe_2O_4$; adsorption

INTRODUCTION

Emerging pollutants are organic compounds introduced into the environment primarily through human activities. These include pharmaceuticals, personal care products, hormones, food additives, pesticides, plasticizers, laundry detergents, disinfectants, surfactants and flame retardants.[1] Pesticides, designed to control pests and insects in agricultural settings, are particularly concerning due to their potential to pollute air, soil, groundwater and surface water ecosystems.[2] If these chemicals are discharged into the atmosphere via agricultural runoff, they can be toxic to humans, fish and birds. Aldrin and dieldrin, in particular, demonstrate significant neurotoxicity due to their impact on chlorinated ion channels, which inhibit sodium entry.[3] These pesticides are also estrogenic and anti-androgenic inhibitors and are known for their bioaccumulation. Aldrin and dieldrin persist in the environment and can be washed from soil into surface water by rainwater. Since these substances do not dissolve in water but adsorb to soil particles, their levels in animal tissues can exceed those found in aquatic ecosystems.[4,5] Aldrin and dieldrin accumulate in sediments of lakes, bays and rivers through runoff.[6] They are chlorinated cyclodienes with broad-spectrum insecticidal properties, acting as poisons through contact, ingestion and inhalation. Aldrin readily transforms into dieldrin, which is recognized as one of the most persistent pesticides.[5,6] The molecular structures of aldrin and dieldrin are illustrated in Fig. 1.

Traditional physical and chemical methods for pollutant removal – such as electrooxidation, incineration, microwave induction and chemical oxidation – not only require extensive and costly infrastructure but also produce byproducts that may be more toxic than the original compounds.[7,8] Microbial degradation, while traditional and environmentally friendly, often encounters nonmicrobial resistance genes that complicate the process.[8] Microbial transformations typically convert aldrin and dieldrin

* *Correspondence to: S Akçağlar, Department of Mechanical Engineering, Faculty of Engineering, Dokuz Eylül University, İzmir, 35390, Turkey, E-mail: sevil.akcaglar@deu.edu.tr*

Department of Mechanical Engineering, Faculty of Engineering, Dokuz Eylül University, İzmir, Turkey

© 2024 The Author(s). *Journal of Chemical Technology and Biotechnology* published by John Wiley & Sons Ltd on behalf of Society of Chemical Industry (SCI).

This is an open access article under the terms of the Creative Commons Attribution-NonCommercial License, which permits use, distribution and reproduction in any medium, provided the original work is properly cited and is not used for commercial purposes.

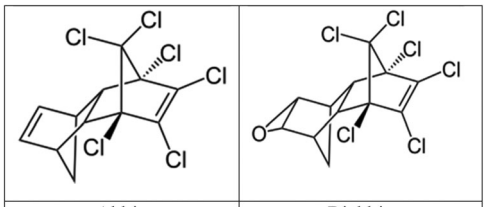


Figure 1. Molecular structures of aldrin and dieldrin.

into sulfate compounds and intermediate chlorinated metabolites rather than achieving complete mineralization to CO_2 and H_2O.[7,9]

Sorption and adsorption techniques, including membrane separation, have shown effectiveness in degrading chlorinated pesticides.[10] For instance, Shrivas *et al.*[11] investigated the adsorption kinetics of aldrin and dieldrin using graphene oxide (GO)–iron oxide (Fe_3O_4) magnetic nanoparticles, achieving removal efficiencies of approximately 77–81% with a 30 min contact time at pH 4.0 at room temperature. Ondijo *et al.*[12] examined the adsorption of these pesticides onto zinc oxide nanoparticles synthesized from *Cissus quadrangularis* leaf extract and activated carbon from maize cobs, achieving adsorption yields of 78–81%.

Heterogeneous photooxidation is an advanced oxidation process utilizing semiconductors as nanocatalysts for water and wastewater purification.[13] Titanium(IV) oxide is a prominent nanocomposite due to its stability, nontoxicity and low cost.[14] It has been reported that incorporating Fe_3O_4 and spinel ferrites like $CoFe_2O_4$, $NiFe_2O_4$ or $ZnFe_2O_4$ into TiO_2 enhances magnetic properties and facilitates catalyst recovery.[11,12]

The application of a TiO_2/GO/$CuFe_2O_4$ nanocomposite for the removal of chlorinated pesticides such as heptachlor, aldrin, heptachlor epoxide, dieldrin, endrin, endosulfan and endrin aldehyde via photocatalysis is relatively limited. Ismael *et al.*[15] reported maximum removal efficiencies of 96.5% and 95.5% for aldrin and dieldrin, respectively, after 14 and 19 min of photodegradation with initial concentrations of 933 and 670 ppb. Esfandian *et al.*[16] studied chlorpyrifos photodegradation using a 0.2 g Cu-doped TiO_2/GO nanocomposite, achieving removal rates of 91.00% and 78.25% under UV and visible light, respectively. Pseudo-first-order kinetics was found to be suitable for the chlorpyrifos photodegradation process, according to the Langmuir–Hinshelwood kinetic model, with rate constants of 0.0301 min^{-1} under UV light and 0.0177 min^{-1} under visible light. Kumar *et al.*[17] investigated the photodegradation of dichlorvos and malathion pesticides from wastewater using a GO–TiO_2 nanocomposite. The maximum photodegradation efficiency for dichlorvos was 74% after 90 min of exposure to 125 W UV irradiation at a pH of 6.0. In contrast, the maximum photodegradation efficiency for malathion was 68% under the same conditions. Additionally, Zangiabadi *et al.*[18] conducted a study on the photodegradation of pesticides, which further complements these findings. The photodegradation of dinoseb and imidacloprid in wastewaters was investigated using a GO/$CuFe_2O_4$–CdS nanocomposite. The maximal pesticide yields were detected as 83% and 86% for initial dinoseb and imidacloprid concentration of 10 mg L^{-1} at a GO/$CuFe_2O_4$–CdS nanocomposite concentration of 100 mg for an irradiation time of 100 min and a pH of 8.0.

Additional studies have explored dye photodegradation using GO–$CuFe_2O_4$–ZnO nanocomposites. Kumar *et al.*[19] achieved 87–89% removal of various dyes such as rhodamine-B and methylene blue (MB) with a nanocomposite concentration of 45 mg L^{-1}. Lin *et al.*[20] investigated the photodegradation of cationic rhodamine-B dye using a CdS/$BiVO_4$ nanocomposite dose at different pH values (5.0, 7.0, 9.6 and 11.5), achieving a maximum dye removal of 87% after 120 min.

Hassan *et al.*[21] investigated the photoremoval of 17 chlorinated pesticides using a Mo–TiO_2/GO/MS nanocomposite for the degradation of persistent chlorinated organic pollutants via UV irradiation. The synthesized nanocomposite was characterized using several analytical techniques, including transmission electron microscopy (TEM), X-ray diffraction (XRD), X-ray photoelectron spectroscopy and UV–visible spectroscopy. The analysis revealed a crystal size of 10 ± 2 nm and an optical absorption enhancement with calculated bandgap energy of 2.75 eV. The highest photocatalytic efficiency of 94.29% was achieved for endrin removal from water under UV illumination after 60 min. The degradation of the pesticides followed pseudo-first-order kinetics.[22]

In a related study, Esfandian *et al.*[16] investigated the photodegradation of chlorpyrifos, a chlorinated pesticide, using a Cu-doped TiO_2/GO nanocomposite. The maximum removal of chlorpyrifos was achieved at a pH of 2, with an irradiation time of 80 min and a photocatalyst dosage of 0.2 g, resulting in 91.00% and 78.25% degradation under UV light and visible light, respectively. Pseudo-first-order kinetics was determined to be suitable for the chlorpyrifos photodegradation process, according to the Langmuir–Hinshelwood model, with rate constants of 0.0301 and 0.0177 min^{-1} for UV light and visible light, respectively.[22]

In a study conducted by Ismael *et al.*,[15] dyes were photodegraded using 28 g of TiO_2/GO/$CuFe_2O_4$ nanocomposite. In another study by Özkal,[23] various antibiotics, including sulfamethoxazole, cefixime, ampicillin, tetracyclines and clarithromycin, as well as *E. coli* bacteria were photodegraded using 15 g of TiO_2/GO/$CuFe_2O_4$ nanocomposite. The study reported low antibiotic photodegradation yields of 77% and bacterial inactivation performances of 76%. Hafeez *et al.*[24] achieved hydrogen gas production at a rate of 35.981 μmol g^{-1} h^{-1} from waste using a TiO_2/GO/$CuFe_2O_4$ nanocomposite.

In the TiO_2/GO/$CuFe_2O_4$ nanocomposite, TiO_2 serves as the primary photocatalytic component, while GO facilitates electron transfer, reducing electron–hole recombination in TiO_2 and enhancing the overall photocatalytic performance. $CuFe_2O_4$ imparts magnetic properties, aiding in the separation of the nanocomposite. Despite the effectiveness of TiO_2 as a photocatalyst with a wide bandgap energy of 3.2 eV for pure anatase, its activity under sunlight is limited due to rapid electron–hole recombination, which reduces photocatalytic efficiency.[25] Metal doping, color sensitization and the use of narrow-bandgap semiconductors improve the photoresponse under sunlight by minimizing electron–hole pair recombination and enhancing the photocatalytic activity for the degradation of organic chlorinated compounds, such as pesticides, in surface water.[26]

The photocatalytic activity of TiO_2 can be significantly enhanced by incorporating ferrites. Specifically, doping TiO_2 with $CuFe_2O_4$ improves its photooxidation performance under sunlight. GO enhances the absorption capacity of certain organic compounds and improves the charge separation efficiency of TiO_2. In other words, GO provides a pathway for electron transfer, which reduces recombination rates in TiO_2 and boosts its photocatalytic activity. Additionally, $CuFe_2O_4$, with its magnetic properties, facilitates the separation of the prepared nanocomposite.

 © 2024 The Author(s).
Journal of Chemical Technology and Biotechnology published by John Wiley & Sons Ltd on behalf of Society of Chemical Industry (SCI).

10974660, 0, Downloaded from https://scijournals.onlinelibrary.wiley.com/doi/10.1002/jctb.7759 by DELIA SPONZA - Turkey Cochrane Evidence Aid , Wiley Online Library on [04/10/2024]. See the Terms and Conditions (https://onlinelibrary.wiley.com/terms-and-conditions) on Wiley Online Library for rules of use; OA articles are governed by the applicable Creative Commons License

In the study reported here, a $TiO_2/GO/CuFe_2O_4$ nanocomposite was utilized to photodegrade two pesticides found in surface waters. The effect of various operational conditions on the photodegradation efficiencies of aldrin and dieldrin was investigated. Recent studies by other researchers have examined the photodegradation of pesticides in wastewater matrices and lake waters. Notable studies include those of Ismael *et al.*,[15] Esfandian *et al.*,[16] Zangiabadi *et al.*,[17] Hassan *et al.*[18] and Kumar *et al.*[21]

The novelty of the work consists of some items given as follows. The reuse of $TiO_2/GO/CuFe_2O_4$ nanocatalyst for 100 cycles with high yields via magnets reduces significantly the cost of the $TiO_2/GO/CuFe_2O_4$ nanocomposite and the utilization of sunlight reduced the energy consumption. The photodegradation of aldrin and dieldrin were not characterized in surface water before and not removed via photocatalysis at high concentrations in neutral pH. No additional chemicals are needed to adjust the pH of the samples. This minimizes significantly the treatment cost. The high bandgap energies of the $TiO_2/GO/CuFe_2O_4$ nanocomposite also provided high photodegradation yields.

The study investigated the effects of various factors on the photodegradation of aldrin and dieldrin, including concentrations (3–9 mg L^{-1} for aldrin and 4–11 mg L^{-1} for dieldrin), nanocomposite concentrations (0.5, 0.9, 1.3 and 1.5 mg L^{-1}), temperatures (20, 30 and 40 °C), pH levels (4, 7 and 9), sunlight intensities (5, 9, 15 and 20 W m^{-2}) and photodegradation times (15, 25, 40 and 60 min). The photodegradation kinetics of both pesticides and the surface properties of the $TiO_2/GO/CuFe_2O_4$ nanocomposite were analyzed using XRD, scanning electron microscopy (SEM), TEM, Fourier transform infrared (FTIR), Raman and UV–visible spectroscopies and energy-dispersive X-ray (EDX) analysis. The study also explored the effect of the TiO_2/GO to $CuFe_2O_4$ ratio on the photocatalytic efficiencies for both pesticides and assessed the reusability of the $TiO_2/GO/CuFe_2O_4$ nanocomposite.

MATERIALS AND METHODS

Production of copper ferrite ($CuFe_2O_4$)

$CuFe_2O_4$ was synthesized using 0.01 mol of $Cu(NO_3)_2{\cdot}6H_2O$ (Merck, Germany, 99% purity) and 0.02 mol of $Fe(NO_3)_3{\cdot}9H_2O$ (Merck, Germany, 99% purity) in equal amounts. After mixing the precipitates of these chemicals, 0.05 mL of 1 mol L^{-1} NaOH (Sigma, St Louis, MO, USA, 99% purity) was added until the pH reached 8.00. The mixture was then incubated at 60 °C for 24 h. Subsequently, the mixture was heated at 820 °C for 150 min. Nanoparticles were obtained using the coprecipitation method.[27]

GO synthesis

For the synthesis of GO, 30 mL of 99% pure H_2SO_4 (Isolab, Ankara, Turkey) and 3.5 mL of 85% pure H_3PO_4 (Merck, Darmstadt, Germany) were mixed in a volume ratio of 8.9:1.2. To this mixture, 0.232 g of graphite powder (Merck, Darmstadt, Germany) was added and stirred. The mixture was stirred for 200 min, and 1.36 g of $KMnO_4$ (Merck, Darmstadt, Germany, 99.0% purity) was gradually introduced into the solution. Subsequently, 220 mL of distilled water and 620 mL of 35% H_2O_2 (Merck, Darmstadt, Germany) were added to the suspension. This mixture was then acidified with HCl (Merck, Darmstadt, Germany), incubated at 65 °C for 35 min and allowed to cool for 12 h. GO was produced using a modified Hummers method.[28]

Production of TiO_2

To produce TiO_2, 30 mL of $Ti(OCH(CH_3)_2)_4$ (Merck, Darmstadt, Germany, 97% purity) was mixed with 120 mL of distilled water. To this solution, 2 mL of NH_4OH (Merck, Darmstadt, Germany) was added and mixed for 15 min. The mixture was then placed in an autoclave at 120 °C for 28 h. Following this, the solution was washed with distilled water and dried at 85 °C for 15 min. TiO_2 nanoparticles were synthesized using the hydrothermal method.[29]

Production of $TiO_2/GO/CuFe_2O_4$ nanocomposite

To synthesize the $TiO_2/GO/CuFe_2O_4$ nanocomposite, 7 g L^{-1} TiO_2, 2.3 g L^{-1} GO and 2.2 g L^{-1} $CuFe_2O_4$ (Merck, Darmstadt, Germany, 98.5% purity) were mixed. To evaluate the effects of the TiO_2/GO to $CuFe_2O_4$ ratio on photodegradation yields, the $TiO_2/GO/CuFe_2O_4$ ratios were varied between 1 and 10 (550 rpm for 3 h).[29]

Physicochemical characterization of $TiO_2/GO/CuFe_2O_4$ nanocomposite

Characterization was performed using an XRD device (D8-ADVANCE, Germany) with Cu Kα radiation (λ = 1.55059 Å), covering a 2θ range of 8° to 100°. The structure of the nanocomposite was examined using field emission SEM (JSM-7800F, JEOL, Japan). TEM was conducted using a 2010F instrument (JEOL, Japan). FTIR analysis was performed using a spectroscopy device (Mettler Toledo, Ankara, Turkey). Raman spectroscopy was conducted with a Raman spectrometer (Edinburgh, UK). UV diffuse-reflectance spectra were collected using a PerkinElmer 330 spectrophotometer (Boston, USA) equipped with a dual-channel diffuse reflectance attachment for UV–visible reflectance spectra. EDX analysis was performed with a Thermo Fisher instrument (USA).

UV–visible diffuse reflectance spectroscopy measurement

UV–visible–near-infrared absorption spectra were recorded using a spectrophotometer with a diffuse reflectance configuration. Measurements were conducted with a V-570 spectrophotometer (Jasco, Japan) equipped with an integrating sphere reflectance unit.

Photodegradation mechanism of $TiO_2/GO/CuFe_2O_4$ nanocomposite

The proposed mechanism for the enhanced photocatalytic degradation of pesticides using the $TiO_2/GO/CuFe_2O_4$ nanocomposite is as follows. Under UV light irradiation, electrons are excited from the valence band to the conduction band of both TiO_2 and $CuFe_2O_4$ semiconductors, creating electron–hole pairs. The conduction band of $CuFe_2O_4$ is more negative than that of TiO_2, leading to the transfer of photoexcited electrons from $CuFe_2O_4$ to TiO_2. Concurrently, the holes in the valence band of TiO_2 migrate to the valence band of $CuFe_2O_4$.

The GO sheets, which are in close contact with both TiO_2 and $CuFe_2O_4$ nanoparticles, act as electron carriers by capturing the photogenerated electrons. This interaction enhances the charge separation efficiency.[30] The pesticide molecules adsorb onto the surface of the $TiO_2/GO/CuFe_2O_4$ nanocomposite, facilitated by interactions between the pesticides and the aromatic regions of GO, as evidenced by the high adsorption capacity of the nanocomposite.

The remaining holes can directly oxidize the adsorbed pesticides, leading to the formation of hydroxyl radicals ($^{\cdot}OH$) and superoxide radicals (O_2^-), which then decompose the pesticides

© 2024 The Author(s).

Journal of Chemical Technology and Biotechnology published by John Wiley & Sons Ltd on behalf of Society of Chemical Industry (SCI).

10974660, 0, Downloaded from https://scijournals.onlinelibrary.wiley.com/doi/10.1002/jctb.7759 by DELIA SPONZA - Turkey Cochrane Evidence Aid , Wiley Online Library on [04/10/2024]. See the Terms and Conditions (https://onlinelibrary.wiley.com/terms-and-conditions) on Wiley Online Library for rules of use; OA articles are governed by the applicable Creative Commons License

into nontoxic products such as CO_2 and H_2O. Consequently, the high photocatalytic activity of the TiO_2/GO/$CuFe_2O_4$ nanocomposite is attributed to its effective charge separation and efficient transfer of photoinduced charge carriers, consistent with the GO-promoted Z-scheme mechanism.

Reusability studies for TiO_2/GO/$CuFe_2O_4$ nanocomposite

Reusability is crucial for the commercial application of photocatalysts. The reusability of the TiO_2/GO/$CuFe_2O_4$ nanocomposite was evaluated through photocatalytic degradation of aldrin and dieldrin under sunlight for 100 cycles. Due to the Fe_2O_4 content, the nanocomposite exhibited magnetic properties, facilitating its removal using a magnetic field. The matrix contained 1.3 mg L^{-1} TiO_2/GO/$CuFe_2O_4$ nanocomposite and 4 mg L^{-1} aldrin and dieldrin, maintained for 25 min. In each cycle, the recovered nanocomposite was isolated from the reaction medium using a magnet. After treatment, approximately 2 L of the nanocomposite mixture was exposed to two magnets (6 cm × 12 cm) placed in the reactor. The nanocomposite was used 100 times, and aldrin and dieldrin concentrations were measured. Additionally, the recovered TiO_2/GO/$CuFe_2O_4$ nanocomposite was weighed to check for mass loss, and its continued usability was verified through 100 cycles.

Photodegradation yields

The photodegradation efficiencies of aldrin and dieldrin were calculated using the following formula:

$$\eta = (1 - C/C_0) \times 100 \quad (1)$$

where C_0 and C are the concentrations of the solution before illumination ($t = 0$) and after illumination of light for t minutes, respectively.

Photocatalytic reactors for photodegradation of aldrin and dieldrin

Photocatalytic experiments were conducted using 5 L glass reactors, constructed by İldam Glass Research Center (Ankara, Turkey). Sunlight measured and adjusted to maintain consistent power between 11:00 a.m. and 4:00 p.m. during the summer was used as the light source for these experiments.

Increasing amounts of the TiO_2/GO/$CuFe_2O_4$ photocatalyst were dispersed into 3000 mL solutions containing varying concentrations of aldrin and dieldrin. The mixtures were stirred continuously under sunlight. Prior to irradiation, the suspensions were stirred in the dark for 1 h to achieve adsorption equilibrium.

At specified intervals, 3 mL samples of the reaction mixture were extracted and centrifuged to remove the photocatalyst. The concentrations of residual pesticides in the samples were determined using gas chromatography (GC). To account for the effects of photolysis and catalysis, blank experiments (without the photocatalyst) were conducted to establish the baseline conversion of the pesticides.

Sunlight measurement

Sunlight intensity was measured using a Solar Light model 450 Microtops II sun-photometer (New York, USA).

Analytical procedure

Aldrin and dieldrin measurements

The concentrations of aldrin and dieldrin were determined using extraction methods followed by GC with mass spectrometry (MS) employing electron capture detection. The detection limits in surface water are approximately 0.001 μg L^{-1} for aldrin and 0.002 μg L^{-1} for dieldrin.[31]

Table 1. Retention times and ion mass/charge of aldrin and dieldrin

	Retention time (min)	Fragmentation ions (mass/charge)
Aldrin	3.528	66, 293, 91
Dieldrin	3.922	79, 81, 263

Separation of the pesticides was achieved using an Agilent J&W DB-5 column (30 m × 0.25 mm internal diameter, 0.25 μm film thickness). For analysis, 2 μL of sample was injected in splitless mode with a purge flow rate of 60 mL min^{-1}, and the injector temperature was set at 250 °C. The temperature program used for the GC analysis was as follows: initial temperature of 100 °C, ramping at 50 °C min^{-1} to 300 °C (held for 1 min). Helium was employed as the carrier gas with a constant flow rate of 2 mL min^{-1}. The interface temperature between GC and MS was maintained at 290 °C. Ions were separated by a quadrupole filter based on their mass-to-charge ratio (m/z). Optimized GC–MS acquisition method parameters for each pesticide are detailed in Table 1.

Chemical oxygen demand (COD) measurements

The COD of surface water was determined according to the methods outlined in Standard Method 5220 (2022) by the American Public Health Association (APHA). COD measurements were conducted using a Spectroquant Nova 30 spectrophotometer (Merck, Darmstadt, Germany).[32]

Total nitrogen (TN) measurements

TN measurements were conducted following the procedure outlined in DIN EN 12260.[33]

Total phosphorus (TP) measurements

TP measurements were carried out using EPA Method 365.1.[34]

Suspended solids (SS) measurements

SS measurements were performed in accordance with Standard Methods 2541-E.[35]

Toxicity testing

Toxicity was assessed using 24-hour-old daphnids to evaluate the impact over 24, 48 and 96 h. For each test, 10 daphnids were added to 100 mL samples. Following specified incubation periods, daphnid immobilization was recorded, and the EC_{50} values were determined.[36,37]

Sampling of surface water

Surface water samples were collected from Gölcük, Ödemiş Lake (İzmir, Turkey), which is intended for use as drinking water prior to treatment. Samples were collected five times a year to measure aldrin and dieldrin concentrations. An automatic water sampler (CSF-48, Endress Hauser, Germany) was used for sampling. The samples were collected in triplicate over a period of 3 h, mixed and then transferred to glass bottles. These samples were stored in a refrigerator at 4 °C until analysis and measurement commenced.

© 2024 The Author(s).

Journal of Chemical Technology and Biotechnology published by John Wiley & Sons Ltd on behalf of Society of Chemical Industry (SCI).

10974660, 0, Downloaded from https://scijournals.onlinelibrary.wiley.com/doi/10.1002/jctb.7759 by DELIA SPONZA - Turkey Cochrane Evidence Aid , Wiley Online Library on [04/10/2024]. See the Terms and Conditions (https://onlinelibrary.wiley.com/terms-and-conditions) on Wiley Online Library for rules of use; OA articles are governed by the applicable Creative Commons License

Measurement of optical properties

Measurement of optical properties via diffuse transmittance and diffuse reflectance measurements of TiO_2/GO/$CuFe_2O_4$ composite suspensions was carried out with an Optronic OL series 750 spectroradiometer. For diffuse measurements, an OL 740-70 integrating sphere reflectance attachment was used. All measurements were carried out in the range between 315 and 415 nm. The path length of the measuring rectangular quartz cuvette was 2 mm. Suspensions with photocatalyst concentrations of 50, 100, 250 and 400 mg·L^{-1} in distilled water were prepared and sonicated for 30 min prior to the measurements.[38]

Calculation of quantum efficiency

Numerous studies agree that the most suitable parameter to compare the intrinsic activity of a photocatalyst is the quantum efficiency (η) when polychromatic radiation is used.[39,40] This parameter can be defined as the ratio of the observed initial molar reaction rate,

$$<r_{CA}(x,t_0)>_{V_R}$$

to the volumetric rate of photon absorption by the photocatalyst,

$$<e^a(x)>_{V_R}$$

both averaged over the reactor volume (Eqn (2)):

$$\eta=[<r_{CA}(x,t_0)>_{V_R}]/[<e^a(x)>_{V_R}] \quad (2)$$

Quantum efficiency η describes the efficiency of the absorbed photons in contributing to the chemical reaction.

Calculation of bandgap energy

The bandgap energy (E_g) can be determined using the Tauc method,[41-43] which involves analyzing the energy-dependent absorption coefficient (α). The relationship is given by:

$$(\alpha\cdot h\nu)^{1/\gamma}=B(h\nu-E_g)(\alpha\cdot h\nu)^{1/\gamma}=B(h\nu-E_g) \quad (3)$$

where h is the Planck constant, ν is the photon frequency, E_g is the bandgap energy and B is a constant. The γ factor depends on the nature of the electron transition and is equal to 1/2 or 2 for direct and indirect transition bandgaps, respectively. To determine E_g, the bandgap energy is usually derived from diffuse reflectance spectra.

According to the Kubelka and Munk theory,[44,45] the reflectance spectra can be transformed into absorption spectra using the Kubelka–Munk function. This function is defined as $F(R_\infty)$, as in Eqn (4):

$$F(R_\infty)=\frac{K}{S}=\frac{(1-R_\infty)^2}{2R_\infty} \quad (4)$$

where $R_\infty = R_{sample}/R_{standard}$ is the reflectance of an infinitely thick specimen, while K and S are the absorption and scattering coefficients, respectively. Putting $F(R_\infty)$ instead of α into Eqn (3) yields the following form:

$$(F(R_\infty)h\nu)^{1/\gamma}=B(h\nu-E_g) \quad (5)$$

RESULTS AND DISCUSSION

Composition of surface water

The characterization of the surface water is summarized in Table 2. The water exhibited a suspension with COD, TN and TP concentrations of 40, 6 and 2 mg L^{-1}, respectively. The concentrations of aldrin and dieldrin in the water samples were approximately 3–9 and 4–11 mg L^{-1}, respectively. These pollutant levels are consistent with findings reported by Rahman and Al-Abadleh[46] and Tarasenko *et al.*,[47] who investigated similar surface waters.

Preliminary studies

Preliminary studies were conducted using a TiO_2/GO/$CuFe_2O_4$ nanocomposite dose of 0.9 mg L^{-1}, under sunlight power of 7 W m^{-2}, at a pH of 6 and a room temperature of 23 °C over a duration of 20 min, based on literature survey findings (Table 3).[48]

In these preliminary studies, the aldrin and dieldrin concentrations in surface water were measured at 4 and 6.2 mg L^{-1}, respectively. The maximum photodegradation yields observed for aldrin and dieldrin were 90% and 91%, respectively (Table 3). These yields are in agreement with those reported by Ismael *et al.*,[15] who observed reductions from initial concentrations of 933.70 and 701.60 ppb to 9.00 and 5.00 ppb, respectively, after 14 and 19 min of photooxidation using a TiO_2/GO/$CuFe_2O_4$ nanocomposite concentration of 20 mg L^{-1}. Duarah *et al.*[49] employed TiO_2/GO/$CuFe_2O_4$, GO, graphitic carbon nitride (g-C_3N_4), molybdenum disulfide (MoS_2) and hexagonal boron nitride (h-BN) nanocomposites for the treatment of organic compounds including aldrin and dieldrin. Their results showed 90% removal yields for dichlorodiphenyl, trichloroethane and methoxychlor; 88% photodegradation efficiencies for aldrin, dieldrin and chlordane; and 84% removal yields for toxaphene, endrin, heptachlor and lindane, using a TiO_2/GO/$CuFe_2O_4$ concentration of 2.5 mg L^{-1} and sunlight power of 85 W m^{-2}. These results are slightly lower than the aldrin and dieldrin yields obtained in our study (99% and 98%, respectively).[49]

Effect of increasing doses of TiO_2/GO/$CuFe_2O_4$ on photooxidation rates of aldrin and dieldrin

Experiments were conducted at a UV power of 8.9 W m^{-2}, a pH of 6.8 and a room temperature of 28 °C for 22 min. The TiO_2/GO to $CuFe_2O_4$ ratio in the TiO_2/GO/$CuFe_2O_4$ nanocomposite was 3.8%. As the TiO_2/GO/$CuFe_2O_4$ nanocomposite concentration increased from 0.5 to 0.9 mg L^{-1} and subsequently to 1.3 mg L^{-1},

Table 2. Characterization of surface water

COD (mg L^{-1})	TN (mg L^{-1})	TP	SS	Aldrin (mg L^{-1})			Dieldrin (mg L^{-1})		
40	6	2	10	3	6	9	4	8	11

Table 3. Photodegradation yields of aldrin and dieldrin in preliminary studies

	Concentration (mg L^{-1})	Removal efficiency (%)
Aldrin	4	90
Dieldrin	6.2	91

© 2024 The Author(s).

Journal of Chemical Technology and Biotechnology published by John Wiley & Sons Ltd on behalf of Society of Chemical Industry (SCI).

10974660, 0, Downloaded from https://scijournals.onlinelibrary.wiley.com/doi/10.1002/jctb.7759 by DELIA SPONZA - Turkey Cochrane Evidence Aid , Wiley Online Library on [04/10/2024]. See the Terms and Conditions (https://onlinelibrary.wiley.com/terms-and-conditions) on Wiley Online Library for rules of use; OA articles are governed by the applicable Creative Commons License

Table 4. Effect of increasing doses of TiO_2/GO/$CuFe_2O_4$ on the photooxidation rates of aldrin and dieldrin

	Aldrin dose (mg L^{-1})			Dieldrin dose (mg L^{-1})		
TiO_2/GO/$CuFe_2O_4$ (mg L^{-1})	3 Removal efficiency (%)	6 Removal efficiency (%)	9 Removal efficiency (%)	4 Removal efficiency (%)	8 Removal efficiency (%)	11 Removal efficiency (%)
0.5	80	80	79	81	80	80
0.9	89	87	87	88	87	87
1.3	99	99	99	99	98	98
1.5	92	91	90	89	89	87

Table 5. Effect of TiO_2/GO to $CuFe_2O_4$ ratio on photooxidation rates of aldrin and dieldrin

	Aldrin (mg L^{-1})			Dieldrin (mg L^{-1})		
TiO_2/GO to $CuFe_2O_4$ ratio in whole TiO_2/GO/Cu Fe_2O_4 (%)	3 Removal efficiency (%)	6 Removal efficiency (%)	9 Removal efficiency (%)	4 Removal efficiency (%)	8 Removal efficiency (%)	11 Removal efficiency (%)
2	94	95	96	93	94	96
4	99	99	100	99	99	99
6	92	93	94	92	92	93
8	91	92	94	90	91	91

aldrin photodegradation yields increased from 79% to 80% to 87% to 89% and then to 99% for aldrin doses of 3, 6 and 9 mg L^{-1}, respectively (Table 4). Similarly, dieldrin photodegradation efficiencies increased from 80% to 81% to 98% to 99% with the increased concentration of TiO_2/GO/$CuFe_2O_4$ (Table 4). The highest photodegradation yields for aldrin and dieldrin were observed at a TiO_2/GO/$CuFe_2O_4$ nanocomposite dose of 1.3 mg L^{-1}. Further increasing the nanocomposite concentration to 1.5 mg L^{-1} resulted in a slight decrease in aldrin and dieldrin photodegradation yields to 90–91% and 87–89%, respectively. This reduction can be attributed to competitive photon absorption, where a smaller amount of energy is absorbed by the TiO_2/GO/$CuFe_2O_4$ nanocomposite. Consequently, lower photooxidation yields were observed due to competition for sunlight photons among multiple metabolites.[50] Duarah *et al.*,[49] Quimbayo *et al.*[51] and Ameta *et al.*[52] reported photodegradation yields of 87% and 90% for pesticides and insecticides using TiO_2/GO/$CuFe_2O_4$ nanocomposites, which were lower than the yields obtained in our study after 1 h of photooxidation at a sunlight power of 90 W m^{-2} with a TiO_2/GO/$CuFe_2O_4$ concentration of 4 mg L^{-1}.

Effect of TiO_2/GO to $CuFe_2O_4$ ratio in TiO_2/GO/$CuFe_2O_4$ nanocomposite

The experimental conditions were set as follows: 1.3 mg L^{-1} TiO_2/GO/$CuFe_2O_4$ nanocomposite dosage, a TiO_2/GO to $CuFe_2O_4$ ratio of 3.8% within the TiO_2/GO/$CuFe_2O_4$ composite, a contact time of 25 min, a pH of 6.9, sunlight power of 8.8 W m^{-2} and a temperature of 27 °C.

When the TiO_2/GO to $CuFe_2O_4$ ratio in the TiO_2/GO/$CuFe_2O_4$ composite was increased from 2% to 4%, the removal efficiencies of aldrin and dieldrin improved from 94% to 96% to 99% to 100% and from 93% to 96% to 99%, respectively. The maximum photodegradation yields for aldrin and dieldrin were achieved at a TiO_2/GO to $CuFe_2O_4$ ratio of 4%, reaching 99–100% and 99%, respectively. However, further increasing this ratio to 6% and 8% resulted in a slight decrease in photodegradation yields. Specifically, aldrin and dieldrin removal efficiencies decreased to 92–94% and 91–94% at 6%, and to 92–93% and 90–91% at 8%, respectively. This decline in efficiency can be attributed to the excessive TiO_2/GO content, which may quench electrons and consequently reduce the overall photodegradation yields (Table 5).[49]

Effect of time on photooxidation rates of aldrin and dieldrin

The optimized conditions for this step were a TiO_2/GO/$CuFe_2O_4$ nanocomposite dose of 1.3 mg L^{-1}, a TiO_2/GO to $CuFe_2O_4$ ratio of 4%, a contact time of 25 min, a pH of 6.9, a sunlight power of 8.9 W m^{-2} and a temperature of 27 °C. Increasing the contact time from 15 to 25 min led to an increase in photooxidation efficiencies for aldrin and dieldrin, from 90% to 91% to 99 to 100% and from 88% to 99% to 99%, respectively (Table 6). The optimum contact time for achieving maximum aldrin and dieldrin yields was 25 min. Extending the contact time further (from 40 to 60 min) resulted in a slight decrease in efficiencies to 91–97% for aldrin and 92–94% for dieldrin. This decrease is attributed to the reduction in the number of active sites, which lowers the photodegradation yields. The equilibrium in photodegradation was achieved within 25 min, with prolonged contact times potentially leading to the inactivation of active sites and reduced adsorption and photodegradation.

Effect of sunlight power on photooxidation rates of aldrin and dieldrin

The optimal operational conditions for this study included a TiO_2/GO/$CuFe_2O_4$ nanocomposite dose of 1.3 mg L^{-1}, a TiO_2/GO to $CuFe_2O_4$ ratio of 4%, a contact time of 25 min, a pH of 6.8 and

© 2024 The Author(s).

Journal of Chemical Technology and Biotechnology published by John Wiley & Sons Ltd on behalf of Society of Chemical Industry (SCI).

10974660, 0, Downloaded from https://scijournals.onlinelibrary.wiley.com/doi/10.1002/jctb.7759 by DELIA SPONZA - Turkey Cochrane Evidence Aid , Wiley Online Library on [04/10/2024]. See the Terms and Conditions (https://onlinelibrary.wiley.com/terms-and-conditions) on Wiley Online Library for rules of use; OA articles are governed by the applicable Creative Commons License

Table 6. Effect of time on photooxidation rates of aldrin and dieldrin

	Aldrin (mg L^{-1})			Dieldrin (mg L^{-1})		
Time (min)	3 Removal efficiency (%)	6 Removal efficiency (%)	9 Removal efficiency (%)	4 Removal efficiency (%)	8 Removal efficiency (%)	11 Removal efficiency (%)
15	90	90	91	88	89	89
25	99	99	100	99	99	99
40	92	97	98	94	94	95
60	91	97	97	92	93	94

Table 7. Effect of sunlight power on photooxidation rates of aldrin and dieldrin

	Aldrin (mg L^{-1})			Dieldrin (mg L^{-1})		
Sun light power (W m^{-2})	3 Removal efficiency (%)	6 Removal efficiency (%)	9 Removal efficiency (%)	4 Removal efficiency (%)	8 Removal efficiency (%)	11 Removal efficiency (%)
5	87	87	86	84	84	85
9	99	99	100	99	99	99
15	90	92	91	91	91	90
20	86	84	86	83	84	85

Table 8. Effect of pH on photooxidation rates of aldrin and dieldrin

	Aldrin (mg L^{-1})			Dieldrin (mg L^{-1})		
pH	3 Removal efficiency (%)	6 Removal efficiency (%)	9 Removal efficiency (%)	4 Removal efficiency (%)	8 Removal efficiency (%)	11 Removal efficiency (%)
4	60	61	62	59	60	61
7	98	98	100	98	98	99
9	50	51	52	50	52	49

varying sunlight powers of 5, 9, 15 and 20 W m^{-2} at a temperature of 27 °C.

In this phase, the effects of different sunlight powers on the removal efficiencies of aldrin and dieldrin were evaluated. As presented in Table 7, the maximum photodegradation efficiencies for aldrin and dieldrin were 99–100% and 99%, respectively, for pesticides concentrations varying between 3 and 9 mg L^{-1} and 4–11 mg L^{-1} when sunlight power was 9 W m^{-2}. Increasing the UV power to 15 and 20 W m^{-2} resulted in a slight decrease in aldrin removal efficiencies to approximately 92%, and a slight reduction in dieldrin photodegradation yields to 83–85% to 83–85%.

These results suggest that increasing sunlight power beyond a certain level does not significantly enhance the photodegradation rates of aldrin and dieldrin. This phenomenon could be attributed to the potential influence of thermoinduced activation, which might alter the degradation mechanism. It is known that both thermooxidation and photooxidation of these pesticides involve similar chemical mechanisms, but with differing effects on the degradation of their functional properties. The lack of further acceleration in photodegradation with higher irradiance aligns with findings by Bigger *et al.*[53]

Effect of pH on photooxidation rates of aldrin and dieldrin

For optimal photooxidation yields, the conditions were set as follows: 1.3 mg L^{-1} TiO_2/GO/$CuFe_2O_4$ nanocomposite dose, a TiO_2/GO to $CuFe_2O_4$ ratio of 4%, a contact time of 25 min and varying pH levels of 4, 7 and 9 with sunlight power of 9 W m^{-2} at a temperature of 30 °C. As presented in Table 8, photooxidation yields were lower under acidic conditions and higher under neutral conditions. At pH 4.0, the photooxidation efficiencies of aldrin and dieldrin were notably low. However, at pH 7, the photooxidation yields improved to 98–100% for aldrin and 98–99% for dieldrin. When the pH was increased to 9, both yields decreased to 50–52% for aldrin and 49–52% for dieldrin. The enhanced photooxidation efficiency at neutral pH can be attributed to the effective generation of hydroxyl radicals, which play a crucial role in the degradation process. Under neutral conditions, photons were absorbed at a wavelength of 260 nm, which is optimal for aldrin and dieldrin. At this wavelength, the photodegradation process

© 2024 The Author(s).

Journal of Chemical Technology and Biotechnology published by John Wiley & Sons Ltd on behalf of Society of Chemical Industry (SCI).

10974660, 0, Downloaded from https://scijournals.onlinelibrary.wiley.com/doi/10.1002/jctb.7759 by DELIA SPONZA - Turkey Cochrane Evidence Aid , Wiley Online Library on [04/10/2024]. See the Terms and Conditions (https://onlinelibrary.wiley.com/terms-and-conditions) on Wiley Online Library for rules of use; OA articles are governed by the applicable Creative Commons License

is more efficient due to reduced competition during photon absorption. Conversely, under alkaline conditions, lower photooxidation yields were observed due to decreased photoquantum efficiency and increased protonation of excited electrons during photodegradation.[54]

Effect of temperature on photooxidation rates of aldrin and dieldrin

For optimal photooxidation yields, the conditions were as follows: 1.3 mg L^{-1} TiO_2/GO/$CuFe_2O_4$nanocomposite dose, a TiO_2/GO to $CuFe_2O_4$ ratio of 4%, a contact time of 25 min, a pH of 7 and a sunlight power of 9 W m^{-2}. The study found that increasing the temperature from 20 to 30 °C resulted in the highest photooxidation efficiencies, with 100% for aldrin and 99% for dieldrin. However, further increasing the temperature to 40 °C led to a slight decrease in yields for both pesticides (Table 9).The highest photooxidation efficiencies for aldrin and dieldrin were observed at 30 °C, achieving removal rates of 100% and 99%, respectively. However, when the temperature was further increased from 30 to 40 °C, a slight decrease in photooxidation yields was noted for both pesticides (Table 9).

As temperature increases during photodegradation, the molecular weight and ultimate mechanical properties of the compounds decrease, while carbonyl groups increase. Photooxidation kinetics generally improves with temperature, as higher temperatures enhance the rate of the oxidation reaction. However, TiO_2 can retard the diffusion of iron ions and oxygen atoms, leading to a slight reduction in oxidation rates at elevated temperatures. At higher temperatures, increased diffusion rates can lead to an accelerated oxidation rate, but this effect reaches a dynamic equilibrium at around 40 °C. During isothermal holding at this temperature, both the promotion and inhibition effects on ion diffusion balance out, resulting in a slower decrease in the oxidation rate. It is also important to consider that elevated temperatures can lead to heterogeneous degradation due to diffusion-limited oxidation, causing a noticeable decrease in the oxidation rate over time. The optimal temperature for photooxidation yields was found to be 30 °C, where the promotion effect of temperature on ion diffusion is most beneficial, leading to slightly higher oxidation rates.[55,56]

Photooxidation kinetics for aldrin and dieldrin

Based on the results of degradation experiments, the photodegradation of the pesticides aldrin and dieldrin follows the Langmuir–Hinshelwood model.[30,57] This kinetic model is expressed by the following:

$$-\frac{dC}{dt} = K_a K_r \frac{C}{1+K_a C} \quad (6)$$

where $-(dC/dt)$ is the photocatalytic oxidation rate, K_r is the photocatalytic oxidation rate constant, K_a is the adsorption equilibrium constant and t is the reaction time. If the product of K_a and C is significantly smaller than 1, the above equation can be simplified to a first-order reaction:

$$-\frac{dC}{dt} = K_a K_r C \quad (7)$$

Consequently, an integrated form of Eqn (7) can be represented as follows:

$$\ln\left(\frac{dC}{dt}\right) = Kt \quad (8)$$

where $K = K_r K_a$ is the apparent rate constant in min^{-1}. The k_{app} value can be obtained by plotting $\ln(C_0/C)$ *versus* t (min). Since pH significantly influences the photodegradation of pesticides on TiO_2/GO/$CuFe_2O_4$, the photodegradation of aldrin and dieldrin was studied at neutral pH, where maximum photodegradation yields were observed. Specifically, for aldrin, the concentration decreased from 6 to 0 mg L^{-1} after a 25 min photodegradation period at neutral pH, as illustrated in Fig. 2.

Based on the variation of zeta potential for TiO_2/GO/$CuFe_2O_4$ as a function of pH, and considering the pK_a of aldrin at pH 7, it was observed that all species, including TiO_2/GO/$CuFe_2O_4$ and aldrin, are negatively charged. This negative charge leads to electrostatic repulsions between pollutant and catalyst, which explains the low level of aldrin adsorption onto TiO_2/GO/$CuFe_2O_4$. The

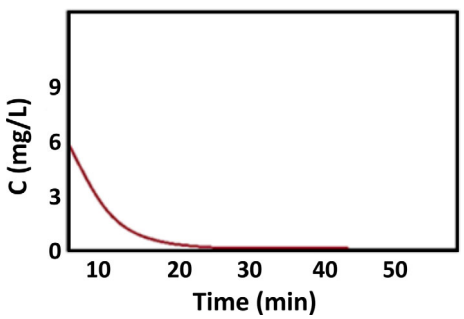


Figure 2. Photocatalytic degradation of aldrin at pH 7 in the presence of 1.3 mg L^{-1} TiO_2/GO/$CuFe_2O_4$ nanocomposite.

Table 9. Effect of temperature on photooxidation rates of aldrin and dieldrin

	Aldrin (mg L^{-1})			Dieldrin (mg L^{-1})		
Temperature (°C)	3 Removal efficiency (%)	6 Removal efficiency (%)	9 Removal efficiency (%)	4 Removal efficiency (%)	8 Removal efficiency (%)	11 Removal efficiency (%)
20	98	98	99	97	97	98
30	99	99	100	98	98	99
40	96	97	97	98	97	94

© 2024 The Author(s).

Journal of Chemical Technology and Biotechnology published by John Wiley & Sons Ltd on behalf of Society of Chemical Industry (SCI).

10974660, 0, Downloaded from https://scijournals.onlinelibrary.wiley.com/doi/10.1002/jctb.7759 by DELIA SPONZA - Turkey Cochrane Evidence Aid , Wiley Online Library on [04/10/2024]. See the Terms and Conditions (https://onlinelibrary.wiley.com/terms-and-conditions) on Wiley Online Library for rules of use; OA articles are governed by the applicable Creative Commons License

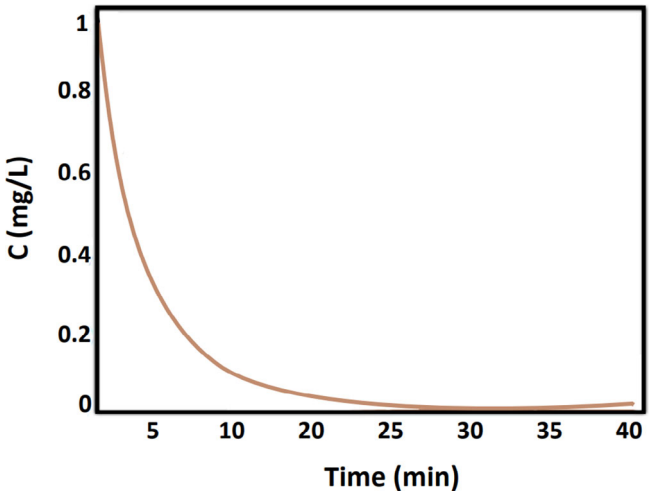


Figure 3. Photocatalytic degradation of dieldrin at pH 7 using a 1.3 mg L^{-1} TiO_2/GO/$CuFe_2O_4$ nanocomposite.

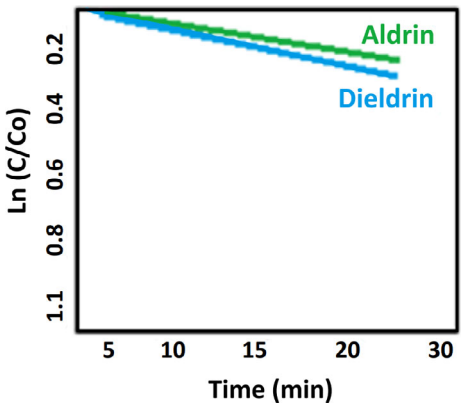


Figure 4. Pseudo-first-order kinetics of aldrin and dieldrin at pH 7 in the presence of 1.3 mg L^{-1} TiO_2/GO/$CuFe_2O_4$.

photodegradation of dieldrin in the presence of 1.3 mg L^{-1} TiO_2/GO/$CuFe_2O_4$ also followed the Langmuir–Hinshelwood model. The photodegradation cycle is illustrated in Fig. 3. The concentration of dieldrin decreased from an initial 1 to 0 mg L^{-1} within 25 min, as depicted in Fig. 3.

To investigate the kinetic parameters, a plot of ln(C_0/C) *versus* irradiation time (t) was constructed. The kinetic study revealed that the photodegradation of aldrin and dieldrin by TiO_2/GO/$CuFe_2O_4$ proceeds more favorably at pH 7. Figure 4 illustrates the evolution of aldrin and dieldrin concentrations based on ln(C_0/C) during the photodegradation process. The pseudo-first-order rate constants were calculated as follows. For aldrin, the pseudo-first-order rate constant (K_1) at pH 7 was 0.05 min^{-1}. For dieldrin, the pseudo-first-order rate constant (K_2) at pH 7 was 0.047 min^{-1}.

These results indicate that the degradation of aldrin and dieldrin by TiO_2/GO/$CuFe_2O_4$ follows pseudo-first-order kinetics, as summarized in Table 10.

During the photodegradation of aldrin and dieldrin, the variation in the chemical structure of these molecules as a function of pH can influence the bond energy and, consequently, the stability of their structures. This effect was documented in previous studies.[58,59] The efficiency of hydroxyl radicals generated from the surface of TiO_2/GO/$CuFe_2O_4$ can be impacted by the structural stability of the pesticides.[60] Under optimal photodegradation conditions, the chlorinated groups within the pesticide molecules undergo degradation, as evidenced by the breakdown of these groups.[61,62]

Table 10. Kinetic parameters of aldrin and dieldrin at pH 7 in the presence of 1.3 mg L^{-1} TiO_2/GO/$CuFe_2O_4$

	Aldrin pH 7	Dieldrin pH 7
K (min^{-1})	0.05	0.047
Photodegradation (%)	99	98

Table 11. Quantum yields of TiO_2/GO/$CuFe_2O_4$ nanocomposite at different concentrations

TiO_2/GO/$CuFe_2O_4$ (mg L^{-1})	Quantum yield, η ($\times 10^2$ mol $einstein^{-1}$)
0.5	1.09
0.9	1.19
1.0	1.65
1.3	2.69
1.5	1.68

Quantum yields of TiO_2/GO/$CuFe_2O_4$ nanocomposite

The highest value of quantum yield (η) was achieved with 1.3 mg L^{-1} TiO_2/GO/$CuFe_2O_4$, recorded as 2.69 × 10^2 mol $einstein^{-1}$. This represents a 100% increase compared to the value obtained with 0.5 mg L^{-1} TiO_2/GO/$CuFe_2O_4$ and a 69% increase compared to 1.0 mg L^{-1} TiO_2/GO/$CuFe_2O_4$ nanocomposite concentration (Table 11). The observed enhancement in quantum yield at 1.3 mg L^{-1} indicates that this concentration is optimal for photocatalytic performance. The improved photocatalytic activity at this concentration can be speculated to result from a reduction in the recombination rate of charge carriers, which is a critical factor in enhancing the efficiency of the photocatalytic process.

Bandgap energy (E_g) of TiO_2/GO/$CuFe_2O_4$ nanocomposite

Figure 5 provides the reflectance spectrum used to analyze the TiO_2/GO/$CuFe_2O_4$ nanocomposite. By transforming this spectrum and plotting it according to Tauc's method, the bandgap energy was calculated, which is found to be 3.31 eV. Understanding these measurements is crucial for evaluating a material's optical and electronic properties, especially considering potential distortions due to material modifications. The steep, linear increase in light absorption with increasing photon energy is a defining feature of semiconductor materials, directly related to their bandgap energy. The presence of significant absorption below the bandgap energy in semiconductors can indeed lead to significant distortions in bandgap determination. Indeed, defects, doping, bulk and surface modifications, and the Urbach tail are all factors that can significantly influence the optical properties of semiconductors and lead to distortions in the determination of the bandgap energy. Factors such as defects, doping, bulk and surface

© 2024 The Author(s).

Journal of Chemical Technology and Biotechnology published by John Wiley & Sons Ltd on behalf of Society of Chemical Industry (SCI).

10974660, 0, Downloaded from https://scijournals.onlinelibrary.wiley.com/doi/10.1002/jctb.7759 by DELIA SPONZA - Turkey Cochrane Evidence Aid , Wiley Online Library on [04/10/2024]. See the Terms and Conditions (https://onlinelibrary.wiley.com/terms-and-conditions) on Wiley Online Library for rules of use; OA articles are governed by the applicable Creative Commons License

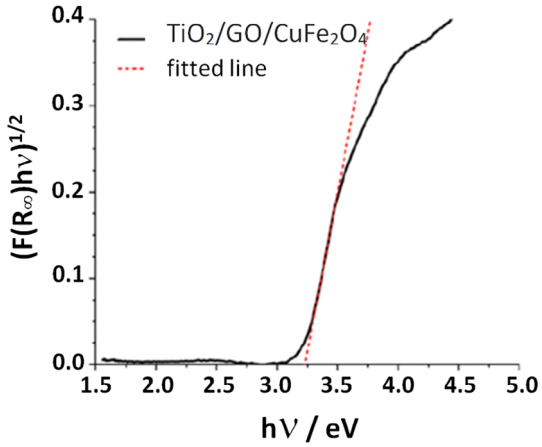


Figure 5. Bandgap energy (E_g) determination of $TiO_2/GO/CuFe_2O_4$ nanocomposite.

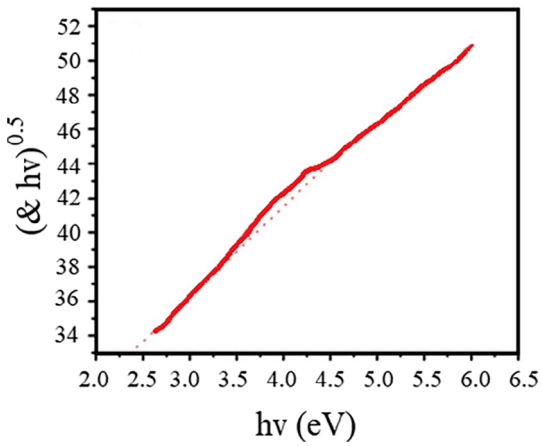


Figure 6. Tauc plot of $TiO_2/GO/CuFe_2O_4$ nanocomposite.

modifications, and the Urbach tail contribute to this phenomenon. Considering these factors and using appropriate analytical methods, one can more accurately assess the bandgap energy and understand the optical behavior of semiconductors. Accurate analysis requires careful consideration of these factors to ensure the correct interpretation of the optical properties and the true bandgap energy of a material. The analysis of the optical properties and bandgap energy of TiO_2/GO composites should be taken into consideration when studying how modifications affect the absorption spectrum. In this case, the presence of GO did not introduce new intrabandgap states, and the Brunauer–Emmett–Teller surface area remained consistent with surface area values of around 57 $m^2\ g^{-1}$.

As aforementioned, according to Kubelka–Munk theory,[44,45] the bandgap energy of the $TiO_2/GO/CuFe_2O_4$ nanocomposite was calculated to be 3.31 eV (Fig. 6) This value is lower than the bandgap energy of pure TiO_2, which is reported to be approximately 0.8 eV in the literature[63-65] (Table 12). The reduction in the bandgap energy of the $TiO_2/GO/CuFe_2O_4$ nanocomposite is a result of the favorable interactions between TiO_2 and GO within the nanocomposite. Specifically, GO enhances the light absorption capabilities of TiO_2 by shifting its absorption into the visible light region. This bandgap narrowing indicates that the $TiO_2/GO/CuFe_2O_4$ nanocomposite can more effectively utilize visible light, contributing to its enhanced photocatalytic performance.

Table 12. Comparison of quantum yields

Catalyst	Quantum yield	
TiO_2	0.8	Abou-Gamra *et al.*[65]
$TiO_2/GO/CuFe_2O_4$ nanocomposite	3.31	This study

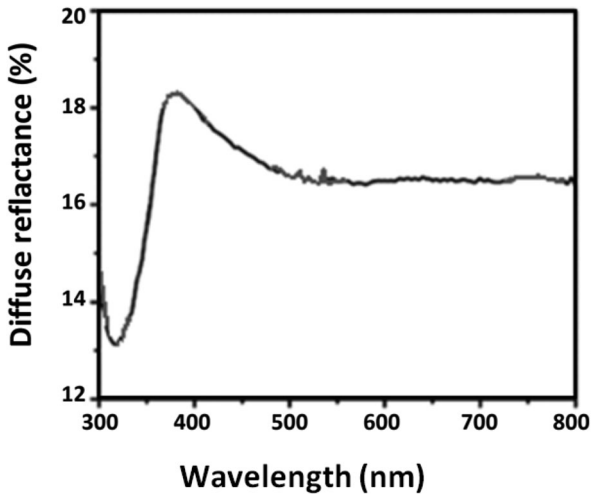


Figure 7. Maximal diffuse reflectance spectrum of $TiO_2/GO/CuFe_2O_4$ nanocomposite.

UV–visible diffuse reflectance spectroscopy: measurement of wavelengths of $TiO_2/GO/CuFe_2O_4$ nanocomposite

Figure 7 shows that the absorption spectrum of the $TiO_2/GO/CuFe_2O_4$ nanocomposite extends into the visible light region. TiO_2 displayed a light response over the range of 350 nm, which is probably due to the band-to-band transition of anatase TiO_2. This extended absorption is attributed to the creation of a new valence band resulting from the hybridization of C_2p and O_2p atomic orbitals.[51]

The photocatalysis process involves two steps: (i) adsorption onto the $TiO_2/GO/CuFe_2O_4$ nanocomposite surface, followed by (ii) photodegradation under UV radiation. $TiO_2/GO/CuFe_2O_4$ was reported as 2.69 eV. A study treated 933 ppb aldrin and 979 ppb dieldrin, achieving lower photodegradation yields (96.5%) compared to the yields (99–100%) obtained in our study.[15] The lower quantum yield values observed for the $TiO_2/GO/CuFe_2O_4$ nanocomposite in our study, with a bandgap energy of 3.31 eV, can be attributed to its relatively higher bandgap compared to some other photocatalysts. For instance, Zhu *et al.*[62] reported a bandgap energy of 2.52 eV for their $ZnFe_2O_4/TiO_2$ nanocomposite, which was used to treat a 2 mg L^{-1} MB dye solution.[61] Despite the lower bandgap energy of the $ZnFe_2O_4/TiO_2$ nanocomposite, the photodegradation efficiency for the MB dye was reported as only 85.7%.[62]

This comparison suggests that while lower bandgap energy generally allows a photocatalyst to absorb a broader range of the visible spectrum, other factors such as quantum yield, charge carrier dynamics and the specific interactions between components in the nanocomposite can significantly influence overall

 © 2024 The Author(s).
Journal of Chemical Technology and Biotechnology published by John Wiley & Sons Ltd on behalf of Society of Chemical Industry (SCI).

10974660, 0, Downloaded from https://scijournals.onlinelibrary.wiley.com/doi/10.1002/jctb.7759 by DELIA SPONZA - Turkey Cochrane Evidence Aid , Wiley Online Library on [04/10/2024]. See the Terms and Conditions (https://onlinelibrary.wiley.com/terms-and-conditions) on Wiley Online Library for rules of use; OA articles are governed by the applicable Creative Commons License

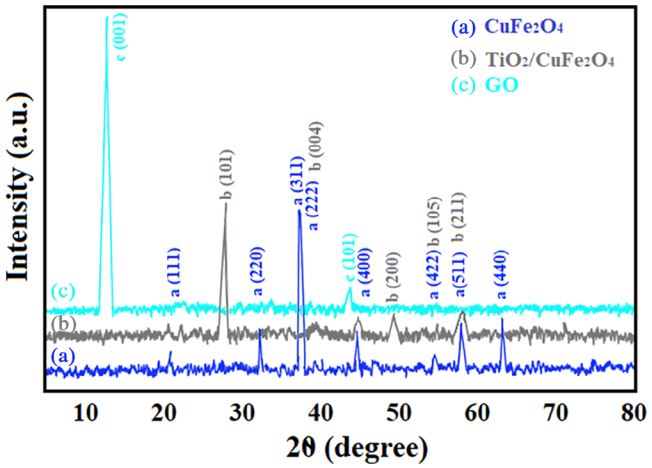


Figure 8. XRD patterns of (a) pure $CuFe_2O_4$, (b) TiO_2/$CuFe_2O_4$ and (c) GO.

photocatalytic performance. In our study, the TiO_2/GO/$CuFe_2O_4$ nanocomposite, with its higher bandgap energy of 3.31 eV, still demonstrated effective photocatalytic activity, indicating that the photocatalytic efficiency is influenced by a combination of factors including quantum yield and the efficiency of charge carrier separation and transfer.

Physicochemical properties of TiO_2/GO/$CuFe_2O_4$

Powder XRD

The XRD patterns for various components are illustrated in Fig. 8. Pure $CuFe_2O_4$ exhibited characteristic peaks at $2\theta = 20.1°$, 32.0°, 37.5°, 39.0°, 44.0°, 55.2°, 58.7° and 63.8°, corresponding to (111), (220), (311), (222), (400), (422), (511) and (440) diffraction planes and pure $CuFe_2O_4$ exhibited crystalline properties (Fig. 8(a)). For TiO_2/$CuFe_2O_4$, peaks were detected at $2\theta = 27.2°$, 39.1°, 48.3°, 54.7° and 57.9°, corresponding to anatase TiO_2 planes (101), (004), (200), (105) and (211). During photodegradation $CuFe_2O_4$/TiO_2 exhibited a crystalline structure (Fig. 8(b)) and pure GO exhibited peaks at $2\theta = 11.8°$ and 43.4° for (001) and (101) planes (Fig. 8 (c)) as reported by Akcaglar.[22] The XRD pattern of the TiO_2/$CuFe_2O_4$ nanocomposite exhibited peaks at $2\theta = 18.1$, 32.2, 43.7, and 49.2, corresponding to (212), (201), (008), and (322) planes (Fig. 8). The XRD pattern of the TiO_2/GO/$CuFe_2O_4$ nanocomposite exhibited maximum signals at $2\theta = 18.1°$, 32.2°, 43.7° and 49.2° corresponding to (212), (201), (008) and (322) (Fig. 9).

FTIR analysis of TiO_2/GO/$CuFe_2O_4$

The FTIR spectrum of the TiO_2/GO/$CuFe_2O_4$ nanocomposite is shown in Fig. 10. Key peaks include 1542 cm^{-1} for O—H groups, a reduction peak at 886 cm^{-1} for the C—O carboxylic group, 1724 cm^{-1} for carbonyl groups, 1222 cm^{-1} for C—O and 1053 cm^{-1} for C—O groups containing oxygen.[49]

Raman spectroscopy

Raman spectroscopy results are presented in Fig. 11. The Raman spectrum for TiO_2/GO/$CuFe_2O_4$ reveals a downshift in both G and D bands compared to GO, indicating reduction of GO.[66] A 2D band at 2699 cm^{-1} is observed, confirming the presence of few-layer graphene sheets in the nanocomposite.[67]

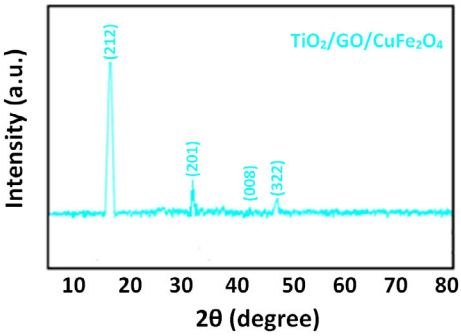


Figure 9. XRD pattern of TiO_2/GO/$CuFe_2O_4$.

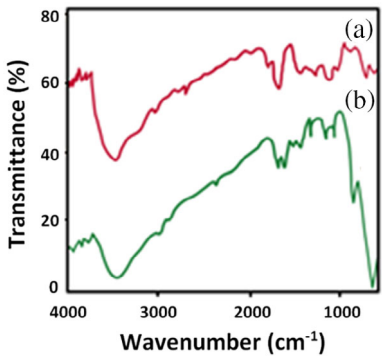


Figure 10. FTIR spectra of (a) GO and (b) TiO_2/GO/$CuFe_2O_4$.

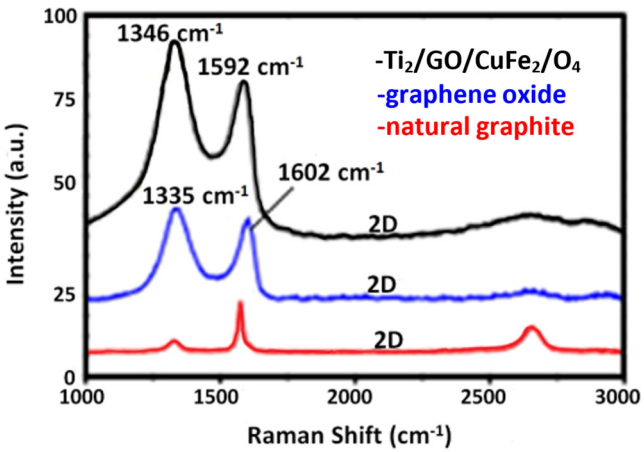


Figure 11. Raman spectra of TiO_2/GO/$CuFe_2O_4$, GO and natural graphite.

Maximum UV absorbances of aldrin and dieldrin

The maximum UV–visible absorbances of aldrin and dieldrin were measured from $\lambda = 220$ to 450 nm. Aldrin and dieldrin displayed maximum absorbances at 342 and 343 nm, respectively (Fig. 12).

SEM and TEM analysis of TiO_2/GO/$CuFe_2O_4$

SEM images (Fig. 13(a)) show that the TiO_2/GO/$CuFe_2O_4$ nanocomposite has some aggregates, displaying non-homogeneous properties. TEM images (Fig. 13(b)) reveal that $TiO_2$and $CuFe_2O_4$ nanoparticles are randomly distributed on GO nanosheets. The low amount of $CuFe_2O_4$/TiO_2 on GO sheets indicates that the nanoparticles are well anchored, with TiO_2 and $CuFe_2O_4$

© 2024 The Author(s).

10974660, 0, Downloaded from https://scijournals.onlinelibrary.wiley.com/doi/10.1002/jctb.7759 by DELIA SPONZA - Turkey Cochrane Evidence Aid , Wiley Online Library on [04/10/2024]. See the Terms and Conditions (https://onlinelibrary.wiley.com/terms-and-conditions) on Wiley Online Library for rules of use; OA articles are governed by the applicable Creative Commons License

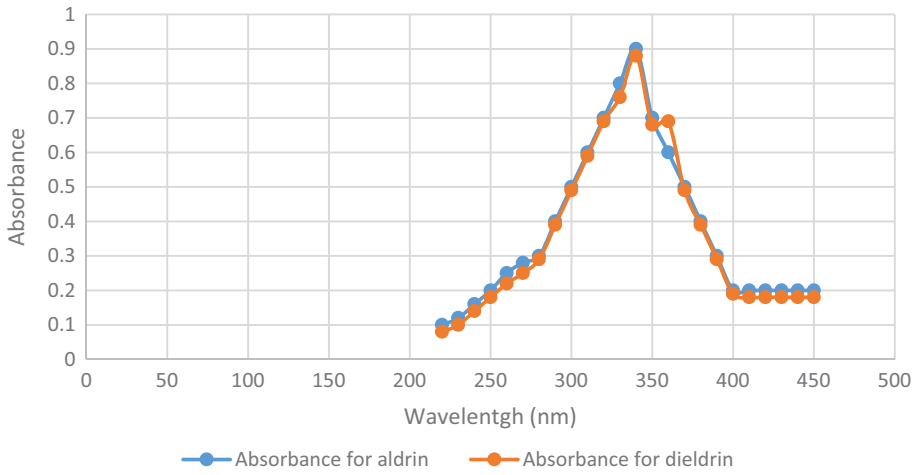


Figure 12. Maximum UV absorbance of aldrin and dieldrin.

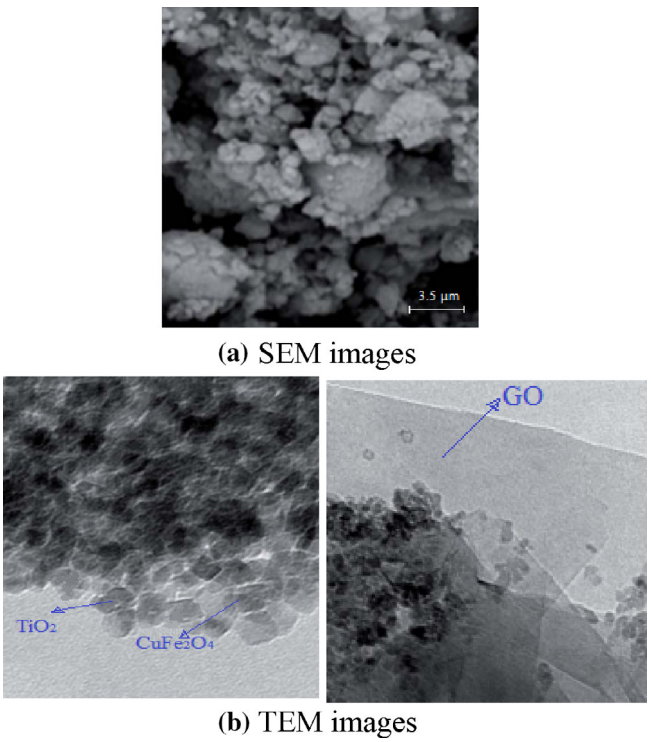


Figure 13. (a) SEM and (b) TEM images of TiO_2/GO/$CuFe_2O_4$ nanocomposite produced under laboratory conditions.

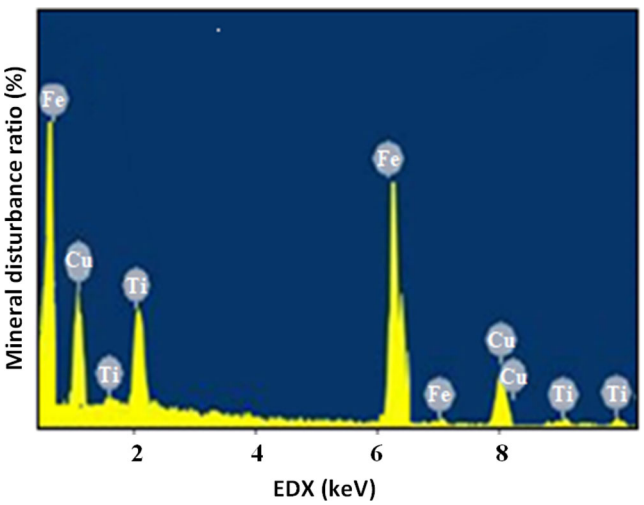


Figure 14. EDX analysis of TiO_2/GO/$CuFe_2O_4$ nanocomposite.

Table 13. Elemental composition in TiO_2/GO/$CuFe_2O_4$ nanocomposite

Elements in TiO_2/GO/$CuFe_2O_4$	Weight (%)
Fe	28.88
Cu	7.21
Ti	7.22
O	56.69

primarily located on the outer surface of GO nanosheets. Well-crystallized single-layer GO was suitable for photodegradation.

EDX analysis of TiO_2/GO/$CuFe_2O_4$

EDX analysis confirmed the presence of key elements such as O, Cu, Ti and Fe in the TiO_2/GO/$CuFe_2O_4$ nanocomposite. The detection of these elements in the EDX analysis confirms the successful synthesis of the GO-based spinel nanocomposite, demonstrating the incorporation of each constituent into the final material. EDX analysis (Fig. 14) confirmed the elemental distribution in the TiO_2/GO/$CuFe_2O_4$ nanocomposite: Cu = 7.21%, Ti = 7.22%, Fe = 8.88% and O = 56.69% (Table 13). The iron-to-copper ratio of 2.02 is close to the theoretical value for $CuFe_2O_4$.

Photodegradation mechanism of aldrin and dieldrin using TiO_2/GO/$CuFe_2O_4$ nanocomposite

The photodegradation of aldrin and dieldrin involves two steps: (i) adsorption onto the TiO_2/GO/$CuFe_2O_4$ surface and (ii) photodegradation under sunlight irradiation. GO enhances pesticide degradation even in the dark (Table 14). The TiO_2/GO/$CuFe_2O_4$ nanocomposite acts as a visible-light-driven photocatalyst due to C–Ti or C–O–Ti bonds, facilitating the separation of photogenerated electron–hole pairs. Furthermore, GO could enhance the e^-/h^+ separation through its p–p stacking between

 © 2024 The Author(s).
Journal of Chemical Technology and Biotechnology published by John Wiley & Sons Ltd on behalf of Society of Chemical Industry (SCI).

10974660, 0, Downloaded from https://scijournals.onlinelibrary.wiley.com/doi/10.1002/jctb.7759 by DELIA SPONZA - Turkey Cochrane Evidence Aid , Wiley Online Library on [04/10/2024]. See the Terms and Conditions (https://onlinelibrary.wiley.com/terms-and-conditions) on Wiley Online Library for rules of use; OA articles are governed by the applicable Creative Commons License

Table 14. 1.3 mg L^{-1} TiO_2/GO/$CuFe_2O_4$ nanocomposite dose, TiO_2/GO to $CuFe_2O_4$ ratio of 4% in TiO_2/GO/$CuFe_2O_4$, at a contact time of 25 min, pH of 7 and sunlight power of 9 W m^{-2}

Presence of relevant component	Dieldrin photodegradation yield (%) (dark)	Aldrin photodegradation yield (%) (dark)	Dieldrin photodegradation yield (%) (under sunlight)	Aldrin photodegradation yield (%) (under sunlight)
TiO_2/$CuFe_2O_4$	23	25	67	68
TiO_2/GO/$CuFe_2O_4$	81	80	99	99
TiO_2	19	20	61	62

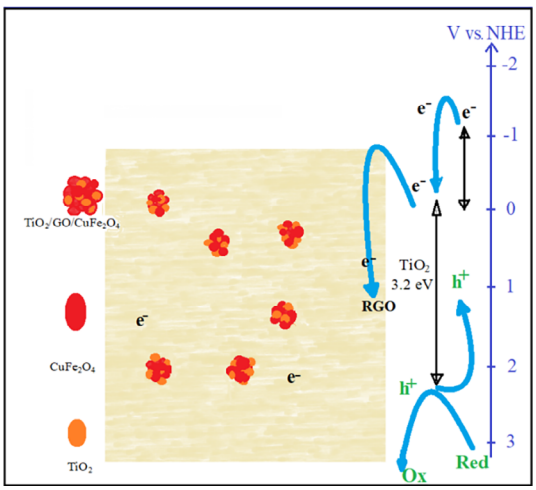


Figure 15. Reaction mechanism of photocatalytic activity in TiO_2/GO/$CuFe_2O_4$ nanocomposite.

pesticides and an aromatic group of GO. $CuFe_2O_4$ alone is almost photocatalytically inactive under solar light irradiation (Table 14). $CuFe_2O_4$ combined with TiO_2/GO leads to an improvement in the photocatalytic performance where 99% of aldrin and dieldrin were decomposed after the same time period. The reasons for these improvements are attributed to the following mechanisms. $CuFe_2O_4$ has a direct bandgap positioned near the optical value of the solar spectrum and a high-energy conduction band, giving the photoelectrons a strong reducing ability. Graphene possesses a remarkable electrical transport property.

Thus, in the $CuFe_2O_4$–TiO_2/GO nanocomposite, a possible reaction mechanism of the observed enhanced photocatalytic activity is proposed (Fig. 15), where the graphene plays a role in conducting electrons, which makes the photocarriers transfer to the surface of GO and improves the separation of the electron–hole pairs and also the photocatalytic efficiency which is the conventional role of GO, as an electron acceptor and transporter, reported in most graphene–semiconductor composites. Under sunlight irradiation, the $CuFe_2O_4$ particles are excited and the photogenerated carriers could easily transfer to the TiO_2 nearby and take part in redox reactions. Therefore, there would be a synergetic effect between $CuFe_2O_4$–TiO_2 nanoparticles and GO, resulting in an appreciable improvement in photodegradation of dieldrin and aldrin compared to TiO_2, $CuFe_2O_4$–TiO_2 and TiO_2/GO. In addition, $CuFe_2O_4$ nanoparticles themselves have excellent magnetic property, which makes the TiO_2/GO/$CuFe_2O_4$ recoverable.

Table 15. Reusability of TiO_2/GO/$CuFe_2O_4$

Run	Aldrin photodegradation yield (%)	Dieldrin photodegradation yield (%)
1	99	99
2	99	99
3	99	99
4	99	99
5	99	99
…	99	99
…	99	99
60	99	99
61	99	99
62	99	99
63	99	99
…	99	99
…	99	99
80	98	98
81	98	98
82	98	98
…	98	98
90	98	98
91	98	98
…	98	98
100	97	97

Recovery and reusability of TiO_2/GO/$CuFe_2O_4$ nanocomposite

To assess the reusability of the TiO_2/GO/$CuFe_2O_4$ nanocomposite, photocatalytic degradation experiments were conducted over 100 cycles with the recovered nanocomposite. Table 15 presents the photodegradation percentages of aldrin and dieldrin after each cycle. From the 1st to the 60th cycle, the photodegradation efficiencies for both aldrin and dieldrin were consistently recorded at 99%. After the 80th cycle, the efficiency slightly decreased to 98%, and after 100 cycles, it was recorded at 97% (Table 15). These results demonstrate that the reusability of the TiO_2/GO/$CuFe_2O_4$ nanocomposite is maintained with minimal decrease in photocatalytic activity over 100 cycles. The ability of the nanocomposite to be reused multiple times without significant loss of performance is crucial for practical applications, as it reduces the cost of photodegradation processes and minimizes environmental impact. In comparison, a study by Ismael *et al.*[15] reported that after 5 cycles, the photodegradation yields of aldrin and dieldrin using a similar nanocomposite decreased from a maximum of 96.5% to 94%. In our study, we observed a high reusability yield of 97% after 100 cycles for the same nanocomposite.

© 2024 The Author(s).

10974660, 0, Downloaded from https://scijournals.onlinelibrary.wiley.com/doi/10.1002/jctb.7759 by DELIA SPONZA - Turkey Cochrane Evidence Aid , Wiley Online Library on [04/10/2024]. See the Terms and Conditions (https://onlinelibrary.wiley.com/terms-and-conditions) on Wiley Online Library for rules of use; OA articles are governed by the applicable Creative Commons License

Furthermore, Zhu *et al.*[62] found that a $ZnFe_2O_4/TiO_2$ nanocomposite, when recycled only 5 times, showed a reduction in MB dye degradation from a maximum of 93.2% to 86.7%.

Results of recent studies on the photodegradation of various pesticides using $TiO_2/GO/CuFe_2O_4$ nanocomposites, along with other relevant research, are summarized in Table 16.

In the study conducted by Ismael *et al.*,[15] the reusability of $TiO_2/GO/CuFe_2O_4$ was evaluated over five cycles, revealing a reduction in aldrin and dieldrin removal efficiency from 96.5% to 94% after the fifth cycle. In contrast, our study demonstrated superior reusability of $TiO_2/GO/CuFe_2O_4$, with a recycling efficiency of 97% after 100 cycles. The maximum photooxidation yields for aldrin and dieldrin achieved in our study ranged from 99% to 100%, surpassing the maximum photodegradation yields of 96.5% reported by Ismael *et al.*[15]

Furthermore, the bandgap energy (E_g) in our study was found to be 3.31 eV, which is higher than the 2.4 eV reported by Ismael *et al.*[15] This higher bandgap energy is associated with increased hydroxyl radical (•OH) production, leading to enhanced photooxidation yields in our study. The kinetics of aldrin and dieldrin photodegradation in our study followed a pseudo-first-order model with rate constants of 0.050 and 0.047 min^{-1}, respectively. In comparison, rate constants of 0.047 and 0.043 min^{-1} were reported by Ismael *et al.*[15] Notably, our study involved higher initial concentrations of aldrin (4 mg L^{-1}) and dieldrin (6.2 mg L^{-1}) compared to the lower concentrations (933 and 670 ppb, respectively) used by Ismael *et al.*,[15] which were assessed at a lower temperature (30 °C).

Recent literature reveals a scarcity of studies focusing on the photodegradation of pesticides using $TiO_2/GO/CuFe_2O_4$ nanocomposites. Among similar studies, Hassan *et al.*[21] reported lower degradation efficiencies of 67% and 49% for aldrin and dieldrin, respectively, using a 20 g Mo-TiO_2/GO/MS nanocomposite concentration over 120 min. This is lower than the yields achieved in our study. However, the nanocomposite dosage and degradation time in their study were significantly higher than those in our study (1.3 mg L^{-1} $TiO_2/GO/CuFe_2O_4$ and 25 min for maximum yields).

Similarly, Esfandian *et al.*[16] and Zangiabadi *et al.*[18] found lower photodegradation yields compared to our study. Esfandian *et al.*[16] reported 98.25% to 91.4% chlorpyrifos degradation with 0.2–0.3 g of Cu-doped TiO_2/GO nanocomposite across a pH range of 2–10. Zangiabadi *et al.*[18] achieved 83% and 86% photodegradation for 10 mg L^{-1} dinoseb and imidacloprid using 16 mg L^{-1} $GO/CuFe_2O_4$–CdS nanocomposite over a pH range of 3 to 11. Our study, utilizing a lower nanocomposite dose (1.3 mg L^{-1}) and achieving maximum yields at a neutral pH of 7.00, represents a more efficient approach. The adjustment of pH to acidic or basic levels, as required in the latter studies, is economically disadvantageous as it increases the treatment costs. Moreover, the cost of using high nanocomposite doses is significant if the nanocomposite is not highly reusable.

Kumar *et al.*[17] investigated the photodegradation of dichlorvos and malathion using 20 mg L^{-1} of GO–TiO_2, reporting degradation yields of 74% and 68%, respectively. This demonstrates a lower efficiency compared to our study, highlighting the effectiveness of our $TiO_2/GO/CuFe_2O_4$ nanocomposite in achieving high pesticide removal efficiencies.

The photodegradation yields for dichlorvos and malathion were found to be 74% and 68%, respectively. In comparing the reaction kinetics, Ismael *et al.*[15] reported pseudo-first-order kinetics for the photodegradation of aldrin and dieldrin, with kinetic constants of 0.0838 and 0.0835 min^{-1}, respectively. In contrast, our study observed pseudo-first-order kinetics with kinetic constants of 0.050 min^{-1} for aldrin and 0.047 min^{-1} for dieldrin. The lower kinetic constants in our study compared to those of Ismael *et al.*[15] may be attributed to differences in the type of kinetic model used and the light source applied during the photodegradation process.

In the studies conducted by Esfandian *et al.*,[16] Zangiabadi *et al.*[18] and Hassan *et al.*[21] UV light was employed, which significantly impacts the overall cost of the process by increasing energy consumption. In contrast, our study utilized sunlight for the photodegradation of aldrin and dieldrin at concentration levels in surface water, as opposed to the UV light used in other studies listed in Table 16, which were performed in wastewater.

Our study employed a lower dosage of $TiO_2/GO/CuFe_2O_4$ (1.3 mg L^{-1}) and achieved high pesticide removal efficiencies within a shorter time frame compared to other studies. An important advantage of the $TiO_2/GO/CuFe_2O_4$ composite is its excellent regeneration capability, allowing it to be reused for multiple cycles of photodegradation without significant loss of efficacy. Regeneration techniques such as pH adjustment desorption agents or thermal treatments were not necessary in our study, as the nanocomposite could be easily separated using a simple magnet. This eliminates additional costs associated with separation and enhances the economic and environmental sustainability of the $TiO_2/GO/CuFe_2O_4$ nanocomposite for wastewater treatment applications.

Given the promising results of the $TiO_2/GO/CuFe_2O_4$ nanocomposite in wastewater treatment, future research should focus on exploring its potential for remediating other pollutants and further optimizing its use in environmental remediation processes.

In the reusability studies, the $TiO_2/GO/CuFe_2O_4$ nanocomposite was successfully reused for 100 cycles, achieving photodegradation yields as high as 97% for aldrin and dieldrin. Notably, there was no sludge production during the photocatalytic treatment of surface water containing aldrin and dieldrin, as these compounds were ultimately photodegraded to CO_2 and water with a yield of 99%. In scenarios where wastewater contained high concentrations of suspended and total solids, these pollutants were also fully degraded to CO_2 and H_2O.

To assess the toxicity of the reused nanocomposite, acute toxicity tests using *Daphnia magna* were conducted on both treated and residual water after 24, 48 and 96 h. No acute toxicity was detected in any of these tests, even after 100 cycles of using the $TiO_2/GO/CuFe_2O_4$ nanocomposite (data not shown).

The maximum photodegradation yields for aldrin and dieldrin were 99% at a $TiO_2/GO/CuFe_2O_4$ concentration of 1.3 mg L^{-1}, with the nanocomposite showing no significant mass loss after reuse. This indicates that the $TiO_2/GO/CuFe_2O_4$ nanocomposite was effectively retained and reused throughout the photodegradation process.

Additionally, quantum yield calculations revealed that η for a 1.00 mg L^{-1} concentration of $TiO_2/GO/CuFe_2O_4$ was 1.65×10^{-2} mol $einstein^{-1}$, while for a 1.3 mg L^{-1} concentration, it was 2.69×10^{-2} mol $einstein^{-1}$ (Table 16). If the nanocomposite dosage were reduced to 1.00 mg L^{-1}, the quantum yield would decrease, leading to reduced photodegradation yields for aldrin and dieldrin. This is because lower quantum yields result in decreased production of OH radicals, which are crucial for effective photodegradation.

The high stability and reusability of the magnetic $TiO_2/GO/CuFe_2O_4$ nanocomposite facilitate its easy separation after the

 © 2024 The Author(s).
Journal of Chemical Technology and Biotechnology published by John Wiley & Sons Ltd on behalf of Society of Chemical Industry (SCI).

10974660, 0, Downloaded from https://scijournals.onlinelibrary.wiley.com/doi/10.1002/jctb.7759 by DELIA SPONZA - Turkey Cochrane Evidence Aid , Wiley Online Library on [04/10/2024]. See the Terms and Conditions (https://onlinelibrary.wiley.com/terms-and-conditions) on Wiley Online Library for rules of use; OA articles are governed by the applicable Creative Commons License

Table 16. Photodegradation of various pesticides using TiO_2/GO/$CuFe_2O_4$ nanocomposites, along with other relevant research

Pesticide	Nano composite	Maximal photooxidation yield (%)	pH range	Temp. (°C)	η ($\times 10^2$ mol einstein^{-1})	E_g (eV)	Reuse cycles	Wavelength (nm)	Pesticide conc. (mg L^{-1})	Nano composite conc. (mg L^{-1})	Photodegradation time (min)	Source	Sunlight power (W m^{-2})	Kinetic constant (min^{-1})	Ref.
	TiO_2/GO/$CuFe_2O_4$														Akçağlar[22]
Aldrin		99–100	4, 7[a], 9	20, 30[a], 40	2.69	3.31	For 79 cycles 99%, for 100 cycles 97%	342	4	1.3	15, 25, 40, 60	Surface water	9	0.05	
Dieldrin		99–99	4, 7, 9	20, 30, 40			For 79 cycles 99%, for 100 cycles 97%	343	4	1.3	15, 25, 40, 60	Surface water	9	0.047	
	TiO_2/GO/$CuFeO_4$														Ismael *et al.*[15]
Aldrin		96.50				2.4	For 1 cycle 96.5%	365	933 ppb	20	14	Waste water		0.0838	
Dieldrin		95.50					For 5 cycle 94%	365	670 ppb	20	19	Waste water		0.0835	
	Cu-doped TiO_2/GO		2							0.2					Esfandian *et al.*[16]
Chlorpyrifos		91.4/78.25	From 2 to 10						10 mg L^{-1}	0.05–0.3 g	20, 40, 60, 80, 100	Waste water	UV and visible	0.0301 and 0.0177	
	GO/$CuFe_2O_4$–CdS		8								100		Visible light		Zangiabadi *et al.*[18]
Ddinoseb		83	From 3 to 11						10	16	10 to 140	Waste water		0.0023	
Imidacloprid		86	From 3 to 11						10		10 to 140	Waste water		0.068	
	Mo–TiO_2/GO/MS		pH 6					362		5.6–20 g	60				Hassan *et al.*[21]
Aldrin		67	From 5 to 9			2.75					40–120	Waste water	UV–visible	0.045	
Dieldrin		49									40–120	Waste water		0.1039	
Endrine		94.29									40–120	Waste water		0.071	
	GO-TiO_2		pH 6							20–200					Kumar *et al.*[17]
Dichlorvos		74	From 2 to 10			1.07			0.5–20 mg L^{-1}		90	Lake	125 W UV	0.032 to 0.036	
Malathion		68	From 2 to 10						0.5–20 mg L^{-1}		90	Lake		0.06 to 0.04	

[a] Values for maximum degradation yields.

© 2024 The Author(s).
10974660, 0, Downloaded from https://scijournals.onlinelibrary.wiley.com/doi/10.1002/jctb.7759 by DELLA SPONZA - Turkey Cochrane Evidence Aid , Wiley Online Library on [04/10/2024]. See the Terms and Conditions (https://onlinelibrary.wiley.com/terms-and-conditions) on Wiley Online Library for rules of use; OA articles are governed by the applicable Creative Commons License

photodegradation process. With chlorinated pesticides being degraded to CO_2 and H_2O with yields up to 99% under optimized conditions, and no sludge production, use of this nanocomposite represents an excellent treatment option.

CONCLUSIONS

A novel TiO_2/GO/$CuFe_2O_4$ nanocomposite was synthesized under controlled laboratory conditions and exhibited significant efficacy in the photodegradation of chlorinated pesticides in surface water. The nanocomposite attained maximum removal efficiencies of 99–100% for aldrin and 99–100% for dieldrin at an initial concentration of 1.3 mg L^{-1}, under a sunlight power of 9 W m^{-2}, at a pH of 7 and at a temperature of 30 °C.

The highest photodegradation efficiencies for aldrin and dieldrin were recorded at 99–100% and 94–96%, respectively, when utilizing a TiO_2/GO to $CuFe_2O_4$ ratio of 4%. Increasing this ratio was observed to reduce the efficiency of pesticide removal.

The TiO_2/GO/$CuFe_2O_4$ nanocatalyst demonstrated exceptional performance in the photoremediation of aldrin and dieldrin, owing to its high reusability, ease of separation from residual waste and significant bandgap energy and quantum yield. The magnetic properties of the TiO_2/GO/$CuFe_2O_4$ nanocomposite facilitate efficient separation and recycling, rendering it a viable and sustainable solution for the treatment of various industrial wastewaters and the photodegradation of other organic chlorinated pollutants.

Consequently, this nanocomposite exhibits considerable potential for broader applications in environmental remediation. The TiO_2/GO/$CuFe_2O_4$ nanocomposite exhibits exceptional performance in the photodegradation of aldrin and dieldrin, achieving removal efficiencies of up to 100%. Its high quantum yield, optimal efficacy under specific conditions, ease of recycling and magnetic properties collectively enhance its effectiveness and practical applicability. This nanocomposite represents a promising candidate for environmental remediation, particularly in the treatment of contaminated surface waters and potentially for other types of pollutants.

DATA AVAILABILITY STATEMENT

Data are available upon reasonable request from the corresponding author.

REFERENCES

1 Yankui T, Yin M, Yang W, Li H and Zhong Y, Emerging pollutants in water environment: occurrence, monitoring, fate, and risk assessment. *Water Environ Res* **1**:1–8 (2019).
2 Alshamsi AMO, Tatan BM, Ashoobi NMS and Mortula MM, Emerging pollutants of water supplies and the effect of climate change. *Environ Rev* **2**:256–277 (2023).
3 Ulloa-Ovares D, Rodríguez-Rodríguez CE, Masís-Mora M and Durán JE, Simultaneous degradation of pharmaceuticals in fixed and fluidized bed reactors using iron-modified diatomite as heterogeneous Fenton catalyst. *Process Saf Environ Prot* **1**:97–107 (2021).
4 ATSDR Agency for Toxic Substances and Disease Registry, Toxicological Profile for Aldrin/Dieldrin, in *Draft for Public Comment: US Department of Health and Human Services*. Public Health Publications USA, Atlanta, GA (2000).
5 Zhang W, Ye Y, Tong Y, Ou L and Hu D, Contribution and loading estimation of organochlorine pesticides from rain and canopy through fall to runoff in an urban environment. *J Hazard Mater* **185**:801–806 (2011).
6 Guan Y, Wang J, Ni H and Zeng EY, Organochlorine pesticides and polychlorinated biphenyls in riverine run off of the Pearl River Delta, China: assessment of mass loading input source and environmental fate. *Environ Pollut* **157**:618–624 (2009).
7 Pang S, Lin Z, Zhang Y, Zhang W, Alansary N and Mishra S, Insights into the toxicity and degradation mechanisms of imidacloprid via physicochemical and microbial approaches. *Toxics* **8**:65 (2020).
8 Zhang W, Pang S, Lin Z, Mishra S, Bhatt P and Chen S, Biotransformation of perfluoroalkyl acid precursors from various environmental systems: advances and perspectives. *Environ Pollut* **272**:115908 (2021).
9 Zhao F, Zhang D, Xu C, Liu J and Shen C, The enhanced degradation and detoxification of chlortetracycline by *Chlamydomonas reinhardtii*. *Ecotoxicol Environ Saf* **196**:110552 (2020).
10 Awfa D, Ateia M, Fujii M, Johnson MS and Yoshimura C, Photodegradation of pharmaceuticals and personal care products in water treatment using carbonaceous-TiO_2 composites: a critical review of recent literature. *Water Res* **142**:26–45 (2018).
11 Shrivas K, Ghosale A, Nirmalkar N, Srivastava A, Singh SK and Shinde SS, Removal of endrin and dieldrin isomeric pesticides through stereoselective adsorption behavior on the graphene oxide-magnetic nanoparticles. *Environ Sci Pollut Res Int* **24**:24980–24988 (2017).
12 Ondijo C, Kengara F and K'Owino I, Synthesis, characterization, and evaluation of the remediation activity of *Cissus quadrangularis* zinc oxide nanoparticle activated carbon composite on dieldrin in aqueous solution. *J Nanotechnol* **2022**:2055024 (2022).
13 Byrne C, Subramanian G and Pillai SC, Recent advances in photocatalysis for environmental applications. *J Environ Chem Eng* **6**:3531–3555 (2018).
14 Ashrafa S, Siddiqab A, Shahidaa S and Qaisar S, Titanium-based nanocomposite materials for arsenic removal from water. A review. *Heliyon* **5**:1577 (2019).
15 Ismael AM, El-Shazly AN, Gaber SE, Rashad MM, Kamel AH and Hassanc SSM, Novel TiO_2/GO/$CuFe_2O_4$ nanocomposite: a magnetic, reusable and visible-light-driven photocatalyst for efficient photocatalytic removal of chlorinated pesticides from wastewater. *RSC Adv* **10**:34806–34814 (2020).
16 Esfandian H, Mirzaei S, Chari AS, Ghadi RA and Moqadam IH, Photocatalytic degradation of chlorpyrifos pesticide in aqueous solution using Cu-doped TiO_2/GO photocatalysis vicinity of UV and visible light. *Mater Sci Eng, B* **305**:117385 (2024).
17 Kumar R, George L, Jun Z and Mukherji S, Photocatalytic activity of graphene oxide-TiO_2 nanocomposite on dichlorvos and malathion and assessment of toxicity changes due to photodegradation. *Chemosphere* **308**:136402 (2022).
18 Zangiabadi M, Saljooqi A, Shamspur T and Mostafavi A, Evaluation of GO nanosheets decorated by $CuFe_2O_4$ and CdS nanoparticles as photocatalyst for the degradation of dinoseb and imidacloprid pesticides. *Ceram Int* **46**:6124–6128 (2020).
19 Kumar P, Govindaraju M, Senthamilselvi S and Premkumar K, Photocatalytic degradation of methyl orange dye using silver (Ag) nanoparticles synthesized from *Ulva lactuca*. *Colloids Surf B* **103**:658–661 (2013).
20 Lin Y, Pan D and Luo H, Hollow direct Z-scheme CdS/$BiVO_4$ composite with boosted photocatalytic performance for RhB degradation and hydrogen production. *Mater Sci Semicond Process* **121**:105453 (2021).
21 Hassan SSM, El-Shazly AN, Ismael AM, Yehia MM, Kamel AH and Rashad MM, Enhanced photocatalytic degradation of chlorinated pesticides and polychlorinated biphenyls using Mo–TiO_2/GO/MS nanocomposite. *Opt Mater* **142**:114084 (2023).
22 Akçağlar S, Adsorption of a paper industry dye (malachite green) using MnO_2-GO nanocomposite. *Fresenius Environ Bull* **31**:9812–9820 (2022).
23 Özkal CB, Synthesis of $CuFe_2O_4$-Ti and $CuFe_2O_4$-Ti-GO nanocomposite photocatalysts using greensynthesized $CuFe_2O_4$: determination of photocatalytic activity, bacteria inactivation and antibiotic degradation potentials under visible light. *J Chem Technol Biotechnol* **97**:1842–1859 (2022).
24 Hafeez Y, Lakhera SK, Karthik P, Anpo M and Neppolian B, Facile construction of ternary $CuFe_2O_4$-TiO_2 nanocomposite supported reduced graphene oxide (rGO) photocatalysts for the efficient hydrogen production. *Appl Surf Sci* **449**:772–779 (2018).
25 El-Sayed A, Atef N, Hegazy AH, Mahmoud KR, Hameed RMA and Allam NK, Defect states determined the performance of dopant-free anatase nanocrystals in solar fuel cells. *Sol Energy* **144**:445–452 (2017).

 © 2024 The Author(s).
Journal of Chemical Technology and Biotechnology published by John Wiley & Sons Ltd on behalf of Society of Chemical Industry (SCI).

10974660, 0, Downloaded from https://scijournals.onlinelibrary.wiley.com/doi/10.1002/jctb.7759 by DELIA SPONZA - Turkey Cochrane Evidence Aid , Wiley Online Library on [04/10/2024]. See the Terms and Conditions (https://onlinelibrary.wiley.com/terms-and-conditions) on Wiley Online Library for rules of use; OA articles are governed by the applicable Creative Commons License

26 Rezk MY, Zeitoun M, El-Shazly AN, Omar MM and Allam NK, Robust photoactive nanoadsorbents with antibacterial activity for the removal of dyes. *J Hazard Mater* **378**:120679 (2019).
27 Deraz NM, Production and characterization of pure and doped copper ferrite nanoparticles. *J Anal Appl Pyrolysis* **82**:212–222 (2008).
28 Toh SY, Loh KS, Kamarudin SK and Daud WRW, Graphene production via electrochemical reduction of graphene oxide: synthesis and characterization. *Chem Eng J* **251**:422–434 (2014).
29 Nabih S, Shalan AE, Serea ESA, Goda M and Sanad MF, Photocatalytic performance of TiO_2@SiO_2 nanocomposites for the treatment of different organic dyes. *J Mater Sci* **30**:9623–9633 (2019).
30 Yari K, Seidmohammadi A, Khazaei M, Bhatnagar A and Leili M, A comparative study for the removal of imidacloprid insecticide from water by chemical-less UVC, UVC/TiO_2 and UVC/ZnO processes. *J Environ Health Sci Eng* **17**:337–351 (2019).
31 Rodrigues JM, Rego ECP, Guimarães EF, Sousa MVB and Monteiro TM, Determination of aldrin purity using a combination of the mass balance approach and quantitative NMR. *J Braz Chem Soc* **26**:869–879 (2015).
32 APHA, *Standard Method for Examination of Water and Waste Water*, 20th edn. American Public Health Association, Washington, DC (1989).
33 DIN EN 12260, Water quality-Determination of nitrogen-Determination of bound nitrogen (TN_b), following oxidation to nitrogen oxides; German version EN Standard by DIN-adopted European Standard 12260 (2003).
34 EPA United States Environmental Protection Agency Method 365.1, Determination of Phosphorus by Semi-Automated Colorimetry, in *Office of Research and Development*, ed. by O'Dell JW. United States Environmental Protection Agency, Cincinnati, OH, 72. US EPA (1993).
35 Standard Methods, Quality Assurance/Quality Control (2022).
36 Daphnia magna OECD 202, Acute Immobilisation Test (Standard Methods) (2022).
37 Wastewater, *American Public Health Association, American Water Works Association*. Water Environment Federation USA, Denver, USA (2022).
38 Tolosana-Moranchel Á, Manassero A, Satuf ML, Alfano OM, Casas JA and Bahamonde A, Influence of TiO_2-rGO optical properties on the photocatalytic activity and efficiency to photodegrade an emerging pollutant. *Appl Catal B* **246**:1–11 (2019).
39 Marugan J, van Grieken R, Cassano AE and Alfano OM, Photocatalysis: fundamentals and perspectives. *R Soc Chem* **14**:367–387 (2016).
40 Manassero A, Satuf ML and Alfano OM, Photocatalytic reactors with suspended and immobilized TiO_2: comparative efficiency evaluation. *Chem Eng J* **326**:29–36 (2017).
41 Davis EA and Mott NF, Conduction in non-crystalline systems V. Conductivity, optical absorption and photoconductivity in amorphous semiconductors. *Philos Mag* **22**:903–922 (1970).
42 Mott NF and Davis EA, *Electronic Processes in Non-Crystalline Materials*. Oxford University Press, Oxford (2012).
43 Makuła P, Pacia M and Macyk W, How to correctly determine the band gap energy of modified semiconductor photocatalysts based on UV–vis spectra. *J Phys Chem Lett* **9**:6814–6817 (2018).
44 Kubelka P and Munk F, A contribution to the optics of pigments. *Z Tech Phys* **12**:593–599 (1931).
45 Brill MH, Vik M and Paul K, *Encyclopedia of Color Science and Technology*. Springer Science+Business Media, New York, USA, pp. 1–3 (2014).
46 Rahman MA and Al-Abadleh HA, Surface water structure and hygroscopic properties of light absorbing secondary organic polymers of atmospheric relevance. *ACS Omega* **3**:15519–15529 (2018).
47 Tarasenko A, Supply A, Kusse-Tiuz N, Ivanov V and Makhotin M, Properties of surface water masses in the Laptev and the east Siberian seas in summer 2018 from in situ and satellite data. *Ocean Sci* **17**: 221–247 (2021).
48 Pabel Y, Ehsan F, Miran MS and Islam MM, Nanocatalysts for the photodegradation of organic pollutants. *Emerg Appl Nanomater* **141**:101–123 (2023).
49 Duarah R, Das P, Boruah PK and Das MN, Current perspective on the development of 2D nanosheets and their composites for photocatalytic degradation of organic pollutants, in *Heterogeneous Nanocatalysis for Energy and Environmental Sustainability*, Vol. 5. Wiley, New Jersey, United States (2022).
50 Wang L and Yu J, Principles of photocatalysis. *Interface Sci Technol* **35**: 1–52 (2023).
51 Quimbayo JM, Ojala S, Urpelainen S, Huuhtanen M and Cao W, Nanostructured photocatalytic materials for water purification, in *Advanced Oxidation Processes for Wastewater Treatment*. IWA Publishing, Boca Raton, FL (2022).
52 Ameta R, Bhatt JP, Avadhanulu MN, Jangid M and Kotharu G, Use of nanomaterials in wastewater treatment. *Sci Nanomater* **8**:1–47 (2022).
53 Bigger SW, Scheirs J and Delatycki O, Effect of sun light intensity on the photooxidation kinetics of high-density polyethylene. *J Polym Sci A: Polym Chem* **30**:2277–2280 (1992).
54 Moradi Z, Jahromi SZ and Ghaedi M, Design of active photocatalysts and visible light photocatalysis. *Interface Sci Technol* **32**:557–623 (2021).
55 Clough RL and Gillen KT, Oxygen diffusion effects in thermally aged elastomers. *Polym Degrad Stab* **38**:47–56 (1992).
56 Pospısil J, Pilar J, Billingham NC, Marek A, Horak Z and Nespurek S, Factors affecting accelerated testing of polymer photostability. *Polym Degrad Stab* **91**:417–422 (2006).
57 Ayoub H, Kassir M, Raad M, Bazzi H and Hijazi A, Effect of dye structure on the photodegradation kinetic using TiO_2 nanoparticles. *J Mater Sci Chem Eng* **5**:31–45 (2017).
58 Ormad MP, Miguel N, Claver A, Matesanz JM and Ovelleiro JL, Pesticides removal in the process of drinking water production. *Chemosphere* **7**:97–106 (2008).
59 Huang F, Chen L, Wang H, Feng T and Yan Z, Degradation of methyl orange by atmospheric DBD plasma: analysis of the degradation effects and degradation path. *J Electrostat* **70**:43–47 (2012).
60 Lü X, Ma H, Zhang Q and Du K, Degradation of methyl orange by UV, O_3 and UV/O_3 systems: analysis of the degradation effects and mineralization mechanism. *Res Chem Intermed* **39**:4189–4203 (2013).
61 El Bakouri H, Morillo J, Usero J and Ouassini A, Natural attenuation of pesticide water contamination by using ecological adsorbents: application for chlorinated pesticides included in European water framework directive. *J Hydrol* **364**:175–181 (2009).
62 Zhu X, Zhang F, Wang M, Ding J, Sun S, Ba J *et al*., Facile synthesis, structure and visible light photocatalytic activity of recyclable $ZnFe_2O_4$/-TiO_2. *Appl Surf Sci* **319**:83–89 (2014).
63 Hamza MA, Abou-Gamra ZM and Ahmed MA, The critical role of Tween 80 as a 'green' template on the physical properties and photocatalytic performance of TiO_2 nanoparticles for rhodamine B photodegradation. *J Mater Sci Mater Electron* **31**:4650–4661 (2020).
64 Nosrati R, Olad A and Shakoori S, Preparation of an antibacterial, hydrophilic and photocatalytically active polyacrylic coating using TiO_2 nanoparticles sensitized by graphene oxide. *Mater Sci Eng C* **80**: 642–651 (2017).
65 Abou-Gamra ZM, Ahmed MA and Hamza MA, Investigation of commercial $PbCrO_4$/TiO_2 for photodegradation of rhodamine B in aqueous solution by visible light. *Nanotechnol Environ Eng* **2**:12 (2017).
66 Stankovich S, Dikin DA, Piner RD, Kohlhaas KA, Kleinhammes A and Jia Y, Synthesis of graphene-based nanosheets via chemical reduction of exfoliated graphite oxide. *Carbon* **45**:1558–1565 (2007).
67 Ferrari AC, Meyer JC, Casiraghi VC, Lazzeri M, Mauri F and Piscanec S, Raman spectrum of graphene and graphene layers. *Phys Rev Lett* **97**:187401–187405 (2006).

10974660, 0, Downloaded from https://scijournals.onlinelibrary.wiley.com/doi/10.1002/jctb.7759 by DELIA SPONZA - Turkey Cochrane Evidence Aid , Wiley Online Library on [04/10/2024]. See the Terms and Conditions (https://onlinelibrary.wiley.com/terms-and-conditions) on Wiley Online Library for rules of use; OA articles are governed by the applicable Creative Commons License

 © 2024 The Author(s).
Journal of Chemical Technology and Biotechnology published by John Wiley & Sons Ltd on behalf of Society of Chemical Industry (SCI).